AGU PUBLICATIONS

JGR

Journal of Geophysical Research: Earth Surface

RESEARCH ARTICLE

10.1002/2014JF003081

Development of topographic asymmetry: Insights from dated cinder cones in the western United States

Luke A. McGuire[1], Jon D. Pelletier[1], and Joshua J. Roering[2]

[1]Department of Geosciences, University of Arizona, Tucson, Arizona, USA, [2]Department of Geological Sciences, University of Oregon, Eugene, Oregon, USA

Key Points:
- Microclimatic effects induced by slope aspect influence hillslope form
- Topographic asymmetry develops on cinder cones throughout the western U.S.
- Spatial variations in vegetation drive differences in sediment transport rates

Correspondence to:
L. A. McGuire,
lmcguire@email.arizona.edu

Citation:
McGuire, L. A., J. D. Pelletier, and J. J. Roering (2014), Development of topographic asymmetry: Insights from dated cinder cones in the western United States, *J. Geophys. Res. Earth Surf.*, *119*, 1725–1750, doi:10.1002/2014JF003081.

Received 2 JAN 2014
Accepted 12 JUL 2014
Accepted article online 18 JUL 2014
Published online 20 AUG 2014

Abstract Topographic asymmetry, that is, differences in the morphology of landscapes as a function of slope aspect, can be used to infer ecohydrogeomorphic feedback relationships. In this study, we document the dependence of topographic gradients and drainage densities on slope aspect and time/age in four Quaternary cinder cone fields in Arizona, Oregon, and California. Cinder cones are particularly useful as natural experiments in geomorphic evolution because they begin their evolution at a known time in the past (many have been radiometrically dated) and because they often have simple, well-constrained initial morphologies. North-facing portions of cinder cones have steeper topographic gradients and higher mean vegetation cover (i.e., Normalized Difference Vegetation Index, or NDVI, values) under current climatic conditions compared with corresponding south-facing portions of cones within each volcanic field. Drainage density is also higher on north-facing portions of cones in three of the four volcanic fields. These differences in topography were not present initially but developed progressively over time, indicating that the asymmetry is a result of post-eruption geomorphic processes. To test alternative hypotheses for the slope-aspect control of topography, we developed a numerical model for cinder cone evolution and a methodology for estimating local paleovegetation cover as a function of elevation, slope aspect, and time within the Quaternary. The numerical model results demonstrate that rates of colluvial transport were higher on south-facing hillslopes in at least three of the four cinder cones fields. Our paleovegetation analysis suggests that in the two Arizona volcanic fields we studied, higher rates of colluvial transport on south-facing hillslopes were the result of greater time-averaged vegetation cover and hence higher rates of sediment transport by floral bioturbation. Our results illustrate the profound impact that relatively small variations in solar insolation can have on landscapes via feedbacks among hydrology, vegetation cover, and sediment transport.

1. Introduction

Understanding how feedbacks among climate, vegetation cover, soil development, and sediment transport shape hillslopes is central to geomorphology. Nearly a century of studies have recognized that slope aspect influences the amount of solar radiation received by a hillslope and that such variations can drive differences in moisture and energy balance that ultimately influence the hydrologic, ecologic, and geomorphic processes that shape hillslopes [e.g., *Russell*, 1931; *Melton*, 1960; *Churchill*, 1981; *Guittierrez-Jurado and Vivoni*, 2013]. The study of topographic asymmetry is potentially powerful because the interactions between climate and hillslope morphology can be examined in detail in settings where nonclimatic variables (e.g., lithology, tectonic forcing) are relatively uniform. However, existing studies demonstrate the difficulty of identifying truly well-controlled study sites where differences in rock structure, lithology, or lateral stream migration, all of which can also result in (or accentuate) the development of topographic asymmetry, are not present [*Bass*, 1929; *Emery*, 1947; *Hack and Goodlett*, 1960; *Melton*, 1960; *Dohrenwend*, 1978].

A number of previous studies have documented topographic asymmetry in the midlatitude regions of North America. Many of these studies have focused on the development of hillslope asymmetry or differences in average topographic gradient as a function of slope aspect. Some studies have documented steeper north-facing hillslopes [e.g., *Pierce and Colman*, 1986; *Branson and Shown*, 1989; *Reeves*, 1996; *Istanbulluoglu et al.*, 2008; *Poulos et al.*, 2012; *West et al.*, 2014], while other studies have documented steeper south-facing hillslopes [e.g., *Churchill*, 1981; *Naylor and Gabet*, 2007; *Burnett et al.*, 2008; *Poulos et al.*, 2012]. *Poulos et al.* [2012] recently developed a method for quantifying hillslope asymmetry at regional-to-continental scales. These authors showed that in midlatitude regions of North America, north- and west-facing hillslopes are

steeper, on average, compared with south- and east-facing hillslopes, respectively. However, they also documented a shift in hillslope asymmetry in the Idaho Batholith from steeper north-facing hillslopes at elevations below 2000 m above mean sea level (a.m.s.l.) to steeper south-facing hillslopes in areas above 2000 m a.m.s.l. In addition, *Poulos et al.* [2012] observed a shift in the orientation of hillslope asymmetry at latitudes above 49°N, with south-facing hillslopes becoming steeper than north-facing hillslopes above this threshold latitude. This reversal in hillslope asymmetry may be the result of present-day variations in erosion mechanisms with climate or of past glacial activity [*Poulos et al.*, 2012]. Such a regional analysis has the potential drawback that structural controls on hillslope asymmetry (which are the dominant factor in driving hillslope asymmetry in some mountain ranges through the development of dip and anti-dip slopes in bedded or banded rocks) may be lumped together with microclimatic controls.

Due to the close connections among sediment transport, water availability, soil development, and vegetation, the changes in hillslope morphology that result from slope-aspect-induced perturbations to a given regional climate may also depend heavily on that regional climate. In water-limited environments, the cooler temperatures and moister soils typical of north-facing hillslopes tend to give rise to more vegetation than the relatively warm and dry south-facing hillslopes. Differences in vegetation and soil properties may influence rates of sediment transport (e.g., bioturbation, freeze-thaw, and slope-wash/fluvial erosion) leading to observable differences in topography over geologic time scales. *Hughes et al.* [2009] argued that a change in vegetation from grass/shrub land to a forested ecosystem led to significantly higher rates of colluvial sediment transport at their study site on the South Island of New Zealand. Rates of colluvial sediment transport, in turn, can lead to changes in soil thickness and rates of soil production, both of which contribute to topographic evolution [*Heimsath et al.*, 1997, 1999, 2001]. Both topography and soil development, which influence water availability, affect the carrying capacity for vegetation.

Despite decades of work on the microclimatic control of hillslope form, we still lack an overarching theory, partly because microclimate can influence different hillslopes in different ways and partly because it is difficult to rule out nonmicroclimatic controls on hillslope asymmetry. *Naylor and Gabet* [2007], in a study of east-west trending valleys in the Bitterroot Range, Montana, found previously glaciated north-facing hillslopes to be less steep than unglaciated south-facing hillslopes. They attributed this difference in mean hillslope gradient to the lateral migration of ridgelines driven by differences in the efficiency of glacial versus nonglacial processes. *Dohrenwend* [1978] investigated hillslope asymmetry in the Gabilan Mesa area of California and found that north-facing hillslopes along east-west-trending valleys are steeper and more vegetated than corresponding south-facing hillslopes. *Dohrenwend* [1978] argued that the geologic history of the Gabilan Mesa minimizes the likelihood of structural controls on the development of hillslope asymmetry and suggested that asymmetries developed as a result of slope-aspect-induced variations in sediment transport mechanisms that led to lateral stream migration and preferential erosion at the foot of north-facing hillslopes. Lateral stream migration may also result from mechanisms other than microclimatically driven variations in sediment transport such as regional tilting [*Leeder and Alexander*, 1987; *Cox*, 1994]. Other studies finding that north-facing hillslopes degrade slower than corresponding south-facing hillslopes attribute this pattern to fewer freeze-thaw cycles [*Pierce and Colman*, 1986; *Branson and Shown*, 1989; *Rech et al.*, 2001; *West et al.*, 2014], lower soil erodibility [*Pierce and Colman*, 1986; *Branson and Shown*, 1989; *Istanbulluoglu et al.*, 2008], and/or lower rates of chemical weathering [*Rech et al.*, 2001] on north-facing hillslopes compared with south-facing hillslopes. In contrast, *Churchill* [1981] examined hillslopes in the badlands of South Dakota and proposed that gentler north-facing hillslopes were the result of higher soil moisture leading to more intense fluvial erosion and frequent mass wasting relative to the drier, steeper south-facing hillslopes. *Burnett et al.* [2008], in a study of canyon slopes eroded into sedimentary rocks in northeastern Arizona, also found south-facing hillslopes to be steep relative to north-facing hillslopes. They attributed these results to a lower weathering rate on south-facing hillslopes resulting from drier conditions.

To better relate topographic asymmetry to slope-aspect-driven ecohydrogeomorphic feedback mechanisms, it is necessary to study landforms that minimize the development of topographic asymmetry through non-ecohydrogeomorphic mechanisms, such as structural controls and changes in lithology, and to examine the sensitivity of any results obtained to changes in regional climate and vegetation type. Lateral stream migration, while it can be driven by ecohydrogeomorphic mechanisms acting on hillslopes [e.g., *Dohrenwend*, 1978], complicates the process of linking asymmetries in hillslope morphology to particular erosion/weathering processes because it is not clear what morphological properties of the hillslopes are a direct result of microclimatically driven variations in sediment transport processes and what properties

are indirectly related to these variations through lateral stream migration. To minimize these complications, we consider the temporal development of asymmetry in the topography, vegetation cover (i.e., biomass), and drainage density of cinder cones located in four basaltic volcanic fields: the San Francisco Volcanic Field (SFVF) in northern Arizona, the Springerville Volcanic Field (SVF) in east-central Arizona, the Newberry Volcanic Field (NVF) in central Oregon, and the Medicine Lake Volcanic Field (MLVF) in northeastern California. We focus on the SFVF, SVF, NVF, and MLVF because each of these fields has large populations of basaltic cinder cones at various stages of development and each contains some cinder cones that have been dated using radiometric techniques [e.g., *Wolfe et al.*, 1987; *Jensen*, 1988; *Conway et al.*, 1998; *Donnelly-Nolan and Lanphere*, 2005; *Fornaciai et al.*, 2012]. Differences in ecology and regional climate among the four volcanic fields enables us to infer relationships among climate, vegetation cover, and rates of colluvial sediment transport across a range of climatic and vegetative environments. Since present-day asymmetries in cinder cone morphology may be relict features that developed under previous climatic conditions, we demonstrate how trends between paleovegetation and slope aspect can be estimated by using present-day vegetation statistics and paleotemperature reconstruction data. We use a landscape evolution model to test various conceptual models for generating the observed asymmetries.

2. Cinder Cone Morphology

Cinder cones are steep, initially conical hills (usually with an interior crater) comprised of scoria (i.e., volcaniclastic debris) that accumulates around a volcanic vent during an eruption. They are often relatively homogeneous in terms of their mineralogical composition and grain size and can be dated using a variety of radiometric [e.g., *Conway et al.*, 1998], stratigraphic [e.g., *Ulrich and Bailey*, 1987; *Hooper and Sheridan*, 1998], and/or morphologic [e.g., *Hooper and Sheridan*, 1998] methods. These properties make cinder cones ideal landforms for quantitative analysis of geomorphic evolution [*Wood*, 1980b; *Dohrenwend et al.*, 1986; *Hooper and Sheridan*, 1998; *Rech et al.*, 2001] and for testing quantitative representations of geomorphic processes [e.g., *Pelletier and Cline*, 2007].

An ideal young cinder cone is radially symmetric with hillslope angles that are approximately equal to the angle of repose for granular material, which can vary depending on grain size and roughness but is typically within the range of 26° to 36° [*Pouliquen*, 1999; *Lamb et al.*, 2013] (Figure 1). Despite these possible variations in initial angle, *Wood* [1980a] examined cinder cones in the SFVF and argued that the angle of repose for volcanic cinder, and therefore the initial cone slope, is not strongly dependent on the particle size distribution. Based on a population of 70 recently emplaced cinder cones ($<$ 0.16 Ma), *Hooper and Sheridan* [1998] found that cinder cones tend to have an average initial slope of $\approx$ 30°.

Still, wind may lead to asymmetries in the initial form of cinder cones by causing preferential deposition of scoria on one side of the vent. For individual cones, such initial asymmetries are only clearly identifiable when they are large. Small, but significant, initial asymmetries may be present but difficult to detect. One way of demonstrating that topographic asymmetry is due to post-eruption geomorphic processes rather than being inherited from initial conditions is to study populations of cones of different ages and demonstrate that a given pattern in the data is statistically insignificant for young cones and statistically significant for older cones. That is the approach we take in this study.

Cinder cones are often emplaced within an interval of time as short as one day and as long as several years [*Wood*, 1980a; *Hasenaka and Carmichael*, 1985]. After formation, cinder cones are modified through a combination of mass wasting, aeolian dust deposition, creep (e.g., rainsplash, bioturbation, freeze-thaw), and slope-wash/fluvial processes that lead to a progressive loss of crater definition, debris-apron development, and gully/valley formation over time. The initial cone soil consists exclusively of coarse cinders, typically centimeter-sized fragments in a loose matrix of fine lapilli [*Wood*, 1980a; *Hooper*, 1994], which limit many transport processes by promoting rapid infiltration and providing minimal potential for water storage [*Hooper*, 1994; *Hooper and Sheridan*, 1998; *Hasenaka and Carmichael*, 1985; *Pelletier and Cline*, 2007]. As such, dry ravel and mass wasting processes are common on recently emplaced cones [*Segerstrom*, 1960; *Pelletier and Cline*, 2007]. Rills can develop on young cones [*Hasenaka and Carmichael*, 1985], but the onset of significant drainage development is often associated with the development of a less permeable soil on the cone surface [*Dohrenwend et al.*, 1986; *Hooper and Sheridan*, 1998]. Soil development, which has been intimately linked to the topographic evolution and hydrologic response of initially permeable basaltic landscapes [*Jefferson et al.*, 2010], may be expected to occur relatively slowly on many young cinder cones.

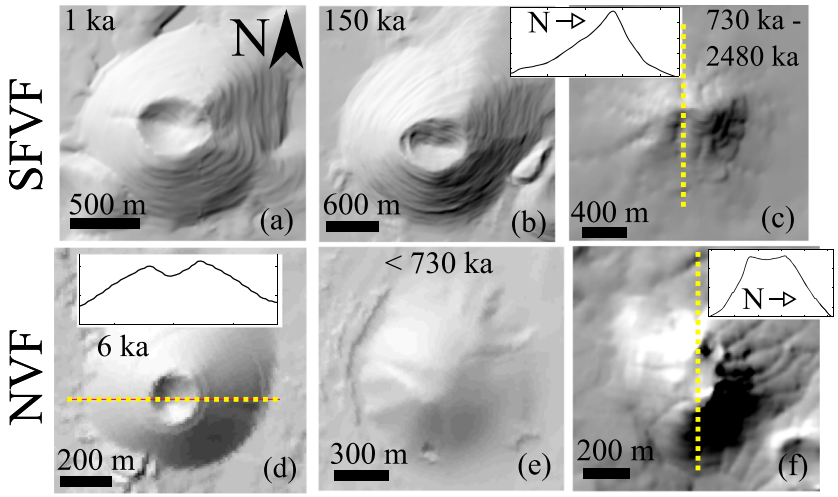

Figure 1. Shaded relief images and topographic profiles illustrating the evolution of cinder cones and the effects of climate on rates of cinder cone degradation. (a) Sunset crater, located in the SFVF, is dated to ≈ 1 ka and maintains steep (> 26°) slopes. (b) Merriam crater in the SFVF, dated to ≈ 150 ka [*Hooper*, 1994], still contains a well-defined central crater and lacks significant drainage development. (c) A highly degraded cinder cone (35.67°N, 111.96°W) within the SFVF, dated to a range of 730–2480 kyr based on magnetic polarity and stratigraphic records [*Hooper*, 1994], lacks a central crater and has a steep north-facing slope. (d) Lava Butte, located within the NVF, has been dated (C14) to approximately 6 ka [*Jensen*, 1988]. (e) An unnamed cinder cone (43.95°N, 121.27°W), less than 730 ka [*MacLeod et al.*, 1995], in the NVF with a poorly defined interior crater. (f) An unnamed, highly degraded cinder cone (43.60°N, 120.74°W) with poorly defined edges.

Hasenaka and Carmichael [1985], in their study of cinder cone morphology within the Michoacán-Guanajuato Volcanic Field of central Mexico, found there to be little to no soil development on cones less than 40 ka and no significant difference in mean or maximum topographic slope angles within the population of cones younger than this age. Particularly in water-limited environments, where in situ weathering of cinders occurs more slowly, the gradual addition of aeolian dust deposits could be critical in promoting greater water storage as the fine particles inhibit infiltration into deeper parts of the cone and evapotranspiration from the shallow subsurface. Greater soil moisture increases vegetation growth in water-limited environments and promotes colluvial transport processes (i.e., frost heave and bioturbation).

Cinder cone degradation may be slow initially due to highly porous soils, but over longer periods of time (i.e., 100–1000 kyr), sediment transport processes lead to progressive degradation and infilling of the central crater, a decrease in maximum hillslope angle [*Wood*, 1980b; *Dohrenwend et al.*, 1986; *Hooper and Sheridan*, 1998], and drainage development [*Dohrenwend et al.*, 1986; *Hooper and Sheridan*, 1998] with increasing age (Figure 1). The rate of cone degradation depends on regional climate [*Wood*, 1980b]. Most cinder cones within the MLVF are dated to less than 500 ka based on stratigraphic relationships and argon dating [*Donnelly-Nolan and Lanphere*, 2005; *Donnelly-Nolan*, 2006] but display a comparable degree of degradation relative to cones in the SFVF and SVF, some of which were emplaced during the Pliocene [*Hooper*, 1994; *Hooper and Sheridan*, 1998]. This similarity in the extent of degradation despite large differences in mean cone age suggests that the rate of degradation is higher, on average, in the MLVF (where the climate is relatively wet) compared with the SFVF and SVF.

Rech et al. [2001] examined the influence of slope aspect on soil development and weathering processes at six cinder cones within the SVF. They found that south-facing hillslopes have higher rates of chemical weathering and greater soil development relative to north-facing hillslopes. *Reeves* [1996] examined a large population of cinder cones within the SVF and found the steepest hillslope angles to be 22.5° on north-facing hillslopes and 18.5° on south-facing hillslopes. Both studies suggest that slope aspect modifies soil development and hillslope morphology on cinder cones. These existing studies did not quantify hillslope-aspect differences in vegetation cover, however, which likely influence, and are influenced by, differences in topography and soil development. Analyzing topographic asymmetry in several different volcanic fields is a first step toward quantifying the ecohydrogeomorphic feedback mechanisms that occur, to some extent, in all landscapes.

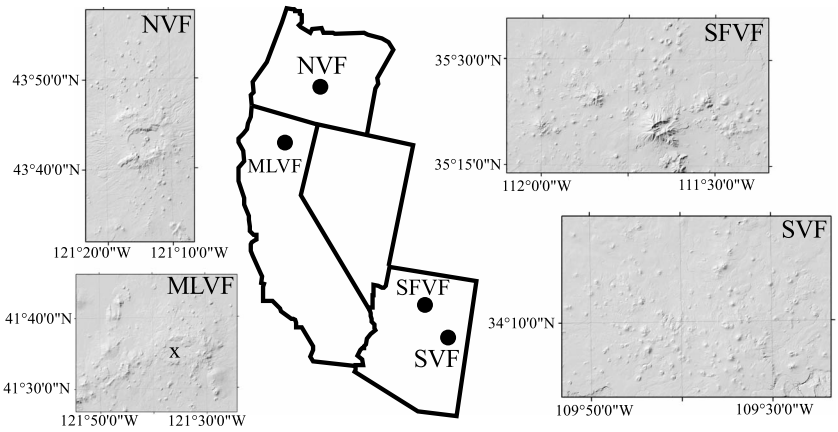

Figure 2. Locations and shaded relief maps for the four study areas, the San Francisco Volcanic Field (SFVF), Springerville Volcanic Field (SVF), Newberry Volcanic Field (NVF), and Medicine Lake Volcanic Field (MLVF). The location of Medicine Lake in the MLVF is also marked.

3. Study Areas

The San Francisco Volcanic Field, located in northeastern Arizona near the southern edge of the Colorado Plateau, contains over 600 volcanic vents, including several hundred basalt cinder cones with a wide range of ages [*Hooper and Sheridan*, 1998] (Figure 2). A group of cinder cones near Ash Fork, located close to the loosely defined, western boundary of the SFVF, are also included within this study area. The SFVF has been active for 6 Myr [*Settle*, 1979; *Conway et al.*, 1998] with the latest eruption (ca. 1120 A.D.) producing a cinder cone at Sunset Crater (Figure 1) [*Moore and Wolfe*, 1987]. The climate in the SFVF can be classified as semi-arid but varies with elevation. Mean annual precipitation is approximately 580 mm near Flagstaff, AZ, but falls to less than 250 mm at the eastern extreme of the SFVF [*PRISM Climate Group*, 2004]. The SFVF contains San Francisco Mountain, a Pliocene to Holocene-aged stratovolcano, which rises to elevations over 3800 m a.m.s.l. Due to the large variations in climate with elevation, the area supports a number of different vegetation communities. However, the majority of the cinder cones are restricted to elevations between 2000 and 2300 m. The mean base elevation over all cinder cones included in this study is 2139 m a.s.l, with 1581 m and 2685 m being the lowest and highest base elevations, respectively. Present-day vegetation within this elevation range includes pinyon pine (*Pinus edulis*) and sagebrush (*Artemisia tridentata*) at lower elevations. Ponderosa pine (*Pinus ponderosa*) forests are found at the higher elevations where precipitation totals tend to be higher [*Hooper and Sheridan*, 1998].

The Springerville Volcanic Field, located in east-central Arizona, covers more than 3000 km^2 and contains hundreds of late Pliocene-Pliestocene basaltic cinder cones [*Condit et al.*, 1989; *Crumpler et al.*, 1994; *Hooper*, 1994; *Rech et al.*, 2001]. The age of nearly all cinder cones range from $\approx$ 2.1 ma to $\approx$ 0.3 ma based on K-Ar dates, magnetic polarity reversal records, and stratigraphic relationships [*Crumpler et al.*, 1994]. More than 50% of cinder cones within the SVF are found between elevations of 2250 m and 2750 m, but elevations across the entire field vary from approximately 1900 m to 3000 m. Mean annual precipitation increases with elevation throughout the area from approximately 250 mm in the lower, northern portion of the field to 750 mm at higher elevations [*PRISM Climate Group*, 2004]. Below 2600 m, vegetation is dominated by ponderosa pine (*Pinus ponderosa*), gambel oak (*Quercus gambelii*), alligator bark juniper (*Juniperus deppeana*), and Douglas fir (*Pseudotsuga menziesii*). Pinyon, sagebrush, and juniper communities tend to dominate at the lowest elevations [*Crumpler et al.*, 1994; *Hooper and Sheridan*, 1998]. Forests of spruce and fir are found along with areas of grasslands at elevations above 2600 m [*Rech et al.*, 2001].

The Newberry Volcanic Field is located south of Bend in central Oregon. Situated on the eastern side of the Cascade Range, it contains over 400 Holocene–Late Pleistocene cinder cones [*MacLeod et al.*, 1995; *Taylor et al.*, 2003; *Hildreth*, 2007]. Most cinder cones are located at elevations between approximately 1500 m to over 1800 m. Mean annual rainfall increases with elevation from roughly 400 mm to 800 mm in higher areas [*PRISM Climate Group*, 2004]. At lower elevations, ponderosa pine (*Pinus ponderosa*) and lodgepole pine (*Pinus contorta*) are common [*Thorson et al.*, 2003]. White fir (*Abies concolor*), mountain hemlock (*Tsuga mertensiana*), and Pacific silver fir (*Abies amabilis*) dominate at the higher elevations [*Thorson et al.*, 2003].

Also included in this study area are several basaltic cinder cones within the nearby Devils Garden Volcanic Field, a Quaternary, basaltic volcanic field located 30 km southeast of Newberry caldera [*Walker et al.*, 1967; *Keith et al.*, 1988; *Chitwood*, 1994].

The Medicine Lake Volcanic Field occupies an area of more than 2200 km^2 in northeast California [*Donnelly-Nolan*, 2006; *Hildreth*, 2007]. It consists of a large shield volcano and central caldera surrounded by hundreds of cinder cones, many of which are composed of basalt and basaltic andesite [*Donnelly-Nolan*, 2006; *Hildreth*, 2007]. The MLVF is located at the southern extent of the Cascade Volcanic Arc, between the Cascade Range and the Modoc Plateau. Elevation ranges from $\approx$ 1500 to 2000 m. Yearly precipitation totals average 750 mm but are lower in the northern and eastern portions of the MLVF and increase to the south and west [*PRISM Climate Group*, 2004]. Modern vegetation near Medicine Lake is dominated by Lodgepole pine (*Pinus contorta*) but also includes Ponderosa (*Pinus ponderosa*) pine, Jeffrey (*Pinus jeffreyi*) pine, sugar (*Pinus lambertiana*) pine, and western white pine (*Pinus monticola*). Red (*Abies magnifica*) and white (*Abies concolor*) fir are present at higher elevations, while Incense cedar (*Calocedrus decurrens*) and western juniper (*Juniperus occidentalis*) can be found at lower elevations and on dry hillslopes [*Starratt et al.*, 2003].

4. Methods

4.1. Analysis of Cinder Cone Morphology and Present-Day Vegetation

Measures of mean and maximum hillslope angles (steepness) and drainage density were compiled from cinder cones within each of the four volcanic fields as a function of age and slope aspect. Measurements of maximum and mean hillslope angles, both of which are used herein, provide slightly different metrics by which to measure hillslope asymmetry. The use of maximum hillslope angle allows for comparison with previous studies [e.g., *Reeves*, 1996] that used this metric and is less sensitive to precise identification of the cone boundaries. Measurements of mean hillslope angle depend on the choice of both the cone boundary and cone center, which are not always clearly defined on old and degraded cones. However, an arbitrary length scale must be chosen over which to compute maximum hillslope angle whereas the length scale over which one computes mean cone slope is set after identifying cone boundaries. We computed the maximum hillslope angle over a length scale of 30 m (i.e., large enough to be resolved in U.S.G.S. 10 m $pixel^{-1}$ Digital Elevation Models (DEMs) yet small enough that it captures the potentially small segment of each cone where the maximum angle is achieved) but trends between maximum hillslope angle and slope aspect do not appear to be sensitive to this choice (i.e., the same trends are observed when calculating maximum hillslope angles over a length scale of 50 m). The maximum hillslope angle was not calculated over a smaller length scale in order to minimize the grid-scale noise present, to some extent, in any digital elevation model (DEM). Differences between the maximum and mean hillslope angles on north- and south-facing sides of cinder cones are both used to evaluate different conceptual models that may explain asymmetries in cinder cone form.

Cinder cones were distinguished from other volcanic features using existing geologic maps [*Walker et al.*, 1967; *Wolfe et al.*, 1987; *Ulrich and Bailey*, 1987; *MacLeod et al.*, 1995; *Donnelly-Nolan*, 2006] and data provided from previous studies [*Hooper*, 1994]. However, since there can be initial asymmetries in the morphology of individual cones due to formation processes, not all cinder cones within the chosen volcanic fields were included in this analysis. For example, breaches caused by lava flows may catastrophically excavate large sections of a cone (Figure 3). Adjacent vents may also influence the development of post-eruption asymmetry (Figure 3). Such cones were not included here because this study focuses on cones that erode progressively over time and lack the complicating effects of interactions with neighboring cones. Cones were also not included in this study if they were too small to be distinguished from spatter cones or too degraded to reasonably estimate cone boundaries. We analyzed a large number of cinder cones (>40) in each volcanic field and performed statistical analyses on cinder cone properties within different age classes in order to determine if differences in hillslope morphology could be linked to post-eruption processes.

DEMs were obtained for every selected cinder cone by projecting 1/3 arc-second elevation data from the National Elevation Dataset (NED) [*Gesch et al.*, 2002; *Gesch*, 2007] onto a grid with a uniform spacing of 10 m. Drainage density was computed for each cone as the sum of all channel lengths divided by the total cone area. Valley heads and drainage networks were identified using contour curvature and flow routing algorithms as described by *Pelletier* [2013]. Mean hillslope angles were computed in each of the four cardinal directions by averaging along radial transects. Maximum hillslope angles were computed along the same

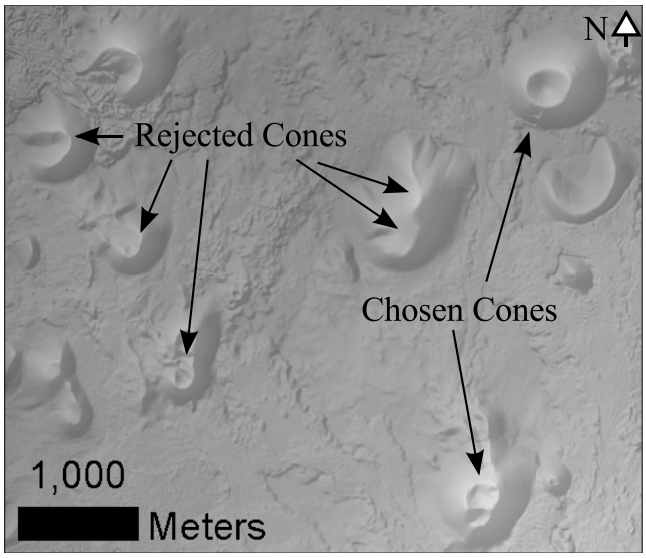

Figure 3. Shaded relief map of lidar-derived digital elevation model for a portion of the NVF. Cinder cones are not included in the study if they have breaches or there are adjacent vents that clearly influence cone evolution.

radial transects. Transects were chosen to ensure that cone hillslope angles were computed from the crater rim, or the cone center if the rim has been completely eroded, to the base of the cone. The mean cone slope was taken as the average of the north, south, east, and west-facing hillslope measurements. Although each cinder cone is contained within a separate DEM that has been cropped to eliminate most of the space surrounding the cone, an additional step was taken to remove areas from the final drainage density statistics that are not on the cone. Locations where the hillslope angle is lower than the minimum of either 5° and 50% of the mean cone slope were not included in the drainage density analysis. We find that this restriction, which is similar to the threshold slope angle of 3.5° used by *Fornaciai et al.* [2012], accurately determines cone boundaries.

Although NED-derived DEMs have been shown to be suitable for similar analyses of cinder cone morphology [*Pelletier and Cline*, 2007; *Fornaciai et al.*, 2012], we estimated the error associated with the use of 10 m pixel^{-1} gridded elevation data through comparison of results with those obtained from airborne lidar-derived DEMs (Figure 4). We derived DEMs for 35 of the cinder cones studied within the NVF from lidar data obtained through the Oregon lidar consortium. Topographic slope and drainage density statistics were computed using the lidar-derived DEMs in the same manner as described earlier for the NED-derived DEMs. To better obtain consistency among all results, final statistics concerning cone morphology within the NVF were computed from NED-derived DEMs even when lidar data were available.

Measurements of mean cone slope were also used as a proxy for cone age in cases where radiometric dates were not available. Cinder cones within the SFVF, SVF, NVF, and MLVF may be placed into broad age groups based on radiometric dating and stratigraphic relationships [*MacLeod et al.*, 1995; *Hooper and Sheridan*, 1998; *Donnelly-Nolan*, 2006]. *Hooper and Sheridan* [1998] examined morphological properties of cinder cones within five age groups in the SFVF and three age groups in the SVF and determined that mean cone slope decreases systematically with time. In section 5, we present similar results for the MLVF to demonstrate that mean cone slope is a reasonable proxy for cone age within this volcanic field. A numerical model, described later in detail, is used to link mean cone slope to cone age within our study areas by quantifying the relationship between time and mean hillslope angle for an idealized cinder cone.

When comparing north- and south-facing hillslopes, cinder cones are separated into two categories, those that are newly emplaced and those that are more degraded, based on approximations of their age (using mean hillslope angle as a proxy for age) relative to other cones within the same volcanic field. A mean cone slope of 20° is chosen to delineate newly emplaced cones from more degraded, older cones. We demonstrate in section 5 that hillslope asymmetry is consistently present on cones with a mean hillslope angle lower than 20° and that cones having a mean slope of 20° in the MLVF, SVF, and SFVF can be dated to approximately 200 ka, 260 ka, and 330 ka, respectively.

Present-day vegetation was quantified as a function of northness within each volcanic field through the Normalized Difference Vegetation Index (NDVI). Northness, η, is defined as the cosine of slope aspect multiplied by the sine of the hillslope angle and ranges from −1 to 1 [*Molotch et al.*, 2005]. Northness is a measure of the extent to which the terrain is north facing and is highly correlated with solar radiation [*Molotch et al.*, 2005; *Sexstone and Fassnacht*, 2014]. NDVI, which is based on the observation that vegetated and nonvegetated surfaces have different albedo characteristics, is commonly used to estimate vegetation cover

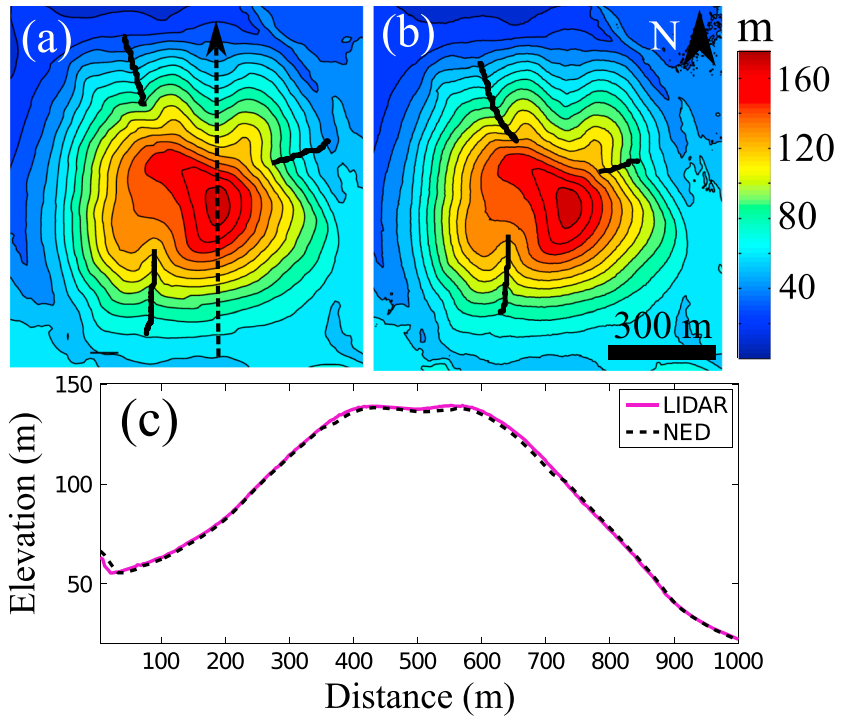

Figure 4. A comparison between lidar-derived and NED-derived DEMs. (a) Topographic contour map (10 m contour intervals) of the NED-derived DEM for an unnamed cinder cone in the NVF (43.85°N, 121.31°W) showing locations (black lines) of identified channels. (b) Topographic contour map (10 m contour intervals) of the lidar-derived DEM for the same cinder cone in the NVF showing locations (black lines) of identified channels. (c) A comparison between topographic transects extracted from the lidar- and NED-derived DEMs.

[*Stensrud*, 2007]. Letting *NIR* and *VIS* denote the values of the spectral reflectance in the near-infrared and visible regions, respectively, NDVI is defined as [*Stensrud*, 2007].

$$NDVI = \frac{NIR - VIS}{NIR + VIS}. \tag{1}$$

For each of the studied cinder cones, NVDI was calculated by extracting high-resolution (1 m) orthoimagery through the United States Geological Survey (U.S.G.S.) National Map Seamless Server (http://seamless.usgs.gov/). These data were chosen because they provide the needed spatial resolution for analyzing vegetation patterns on cinder cones. The orthoimages were acquired during the agricultural growing season as a part of the National Agriculture Imagery Program (NAIP) and represent the state of the vegetation at that time. Calculations of NDVI derived from these data are therefore representative of the state of the vegetation during the growing season. NDVI was cast as a function of northness by interpolating topographic slope and slope aspect information, derived from DEMs, to match the location of pixels on the orthoimagery. NDVI is not a direct measure of biomass and its value may also reflect the health of vegetation, but for the purposes of this study we associated higher values of NDVI with greater biomass.

In addition, we quantified the extent to which an environment is water-limited through the use of a precipitation effectiveness index, *PE*. The *PE* index is a measure of the availability of moisture to vegetation and is defined by *Thornthwaite* [1931] as

$$PE = \sum_{i=1}^{12} 115 \left(\frac{\max(P_i, 0.5)}{\max(T_i, 28.4) - 10} \right)^{10/9}, \tag{2}$$

where P_i and T_i denote total precipitation (inches) and average temperature (°*F*) in month *i*, respectively. We obtained monthly averages of precipitation and maximum and minimum temperature from PRISM data [*PRISM Climate Group*, 2004]. Average monthly temperature was taken as the average of monthly maximum and minimum temperatures. Typical values of *PE* range from less than 15 in the arid portions of Arizona to more than 100 in the more humid regions of coastal California. The average values of *PE* for the SFVF, SVF, NVF, and MLVF are 45 $(\text{in}/°\text{F})^{10/9}$, 58 $(\text{in}/°\text{F})^{10/9}$, 72 $(\text{in}/°\text{F})^{10/9}$, and 110 $(\text{in}/°\text{F})^{10/9}$, respectively.

4.2. Estimates of Paleovegetation

Although we can quantify present-day vegetation cover using NDVI, major changes in vegetation have accompanied climate change following the Pleistocene-Holocene transition near our study sites in Oregon and California [e.g., *Hakala and Adam*, 2004; *Colman et al.*, 2004] as well as Arizona [e.g., *Anderson*, 1993; *Anderson et al.*, 2000]. *Hakala and Adam* [2004] used pollen and sediment data from Grass Lake, located 50 km west of the MLVF at an elevation of ≈ 1500 m, to infer that the surrounding area was above the upper tree line at least twice during the last 40 kyr. The current upper tree line on nearby Mount Shasta is roughly 2500 m a.m.s.l. *Hakala and Adam* [2004] proposed that vegetation changes within the southern Cascade Range have occurred in response to climate change on submillennial time scales near our study site in the MLVF, indicating a complex relationship between vegetation and climate within this region. To our knowledge, there is little paleovegetation data available for the NVF. In contrast, analysis of packrat midden and lake sediment data in the southern Colorado Plateau indicate that paleovegetation may be quantified, to first order, as a shift in the elevation ranges of different vegetation communities, with present-day vegetation similar to vegetation that existed approximately 1.0 km lower in elevation at Last Glacial Maximum (LGM) [*Betancourt*, 1990; *Cole*, 1990; *Anderson*, 1993; *Anderson et al.*, 2000].

To honor the dominant role of elevation in controlling vegetation communities both now and in the late Quaternary, we developed a methodology for estimating the relationship between paleovegetation and elevation for north- and south-facing hillslopes within the two Arizona study sites based on elevation shifts that track Quaternary climatic (i.e., temperature) changes. This analysis is not directly applicable to the MLVF and NVF study areas, but an in-depth analysis of paleovegetation in the Arizona volcanic fields may still provide valuable insight and field-testable hypotheses that are more generally applicable. Our method is based on the idea that the cooler and wetter conditions that dominated during the majority of the Pleistocene are well represented by present-day climates at higher elevations and that temperature and moisture variations across elevation gradients lead to associated changes in vegetation cover. Specifically, we estimated the relative vegetation cover on north- versus south-facing hillslopes during the Pleistocene in the SFVF and SVF by first quantifying the relationship between present-day NDVI and slope aspect as a function of elevation and then shifting this curve down in elevation by an amount proportional to the temperature difference relative to the modern. To perform this analysis, we selected a large region of approximately 500 km^2 within the SFVF that contains San Francisco Mountain (the tallest peak in Arizona and the only location currently above treeline). We consider this analysis to also apply to the SVF given its relatively close proximity to the SFVF (SVF is ≈ 200 km to the southeast of SFVF) and the similarities in present-day climate and vegetation type between the two sites. NDVI was computed over the entire region at a 10 m scale, and mean NDVI on north- and south-facing hillslopes were then computed separately and cast as functions of elevation.

Temperature estimates relative to present, derived from deuterium concentrations at Vostok, Antarctica [e.g., *Petit et al.*, 1999], indicate that atmospheric temperatures may have been as much as 7–9°C cooler than today during the LGM. More specifically, paleotemperature estimates derived from noble gas concentrations in groundwater suggest temperatures during the LGM were ≈ 6°C cooler than present in the southern Colorado Plateau [*Phillips et al.*, 1986; *Stute et al.*, 1995; *Zhu and Kipfer*, 2010]. Assuming a lapse rate of 6° C km^{-1}, this temperature difference corresponds to an apparent change in elevation of approximately ~1000 m. Modern lapse rates in the southern Colorado Plateau are roughly 5–6° C km^{-1} [*Phillips et al.*, 1986; *Stute et al.*, 1995]. Therefore, one can expect the vegetation type/density found today at an elevation of ~3000 m to be similar to that found at ~2000 m in elevation during the last glacial maximum. This agrees well with studies of paleovegetation in the southern Colorado Plateau that find present-day elevation zones of vegetation communities may have shifted up in elevation by more than 800 m since the late Wisconsin (21.0–10.4 kyr B.P.) [*Cole*, 1990; *Anderson*, 1993; *Anderson et al.*, 2000]. More importantly, present-day variations in biomass with slope aspect at ≈ 3000 m in elevation can be used to approximate the variations in biomass with slope aspect that existed at ≈ 2000 m during the last glacial maximum. By using temperature deviations from present as a scaling variable, we do not wish to imply that paleovegetation changes relative to today depend only on temperature. Temperature does directly influence water availability in soils (via evapotranspiration), but more broadly aridity is a function of both temperature and precipitation. In the SW U.S., however, past temperatures and precipitation values at a given elevation are inversely related [*Wagner et al.*, 2010] such that temperature alone provides a useful proxy since high-resolution time series are readily available.

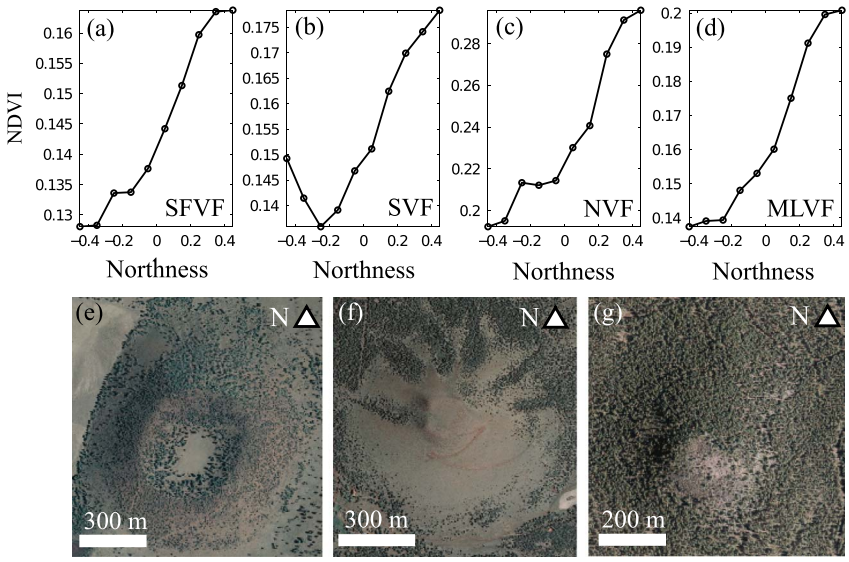

Figure 5. NDVI, computed from high-resolution orthoimages, is shown as a function of northness within each of the four study areas. NDVI appears to be an increasing function of northness in the (a) SFVF, (b) SVF, (c) NVF, and (d) MLVF. (e) Orthoimage of a cinder cone (35.39°N, 121.57°W) in the SFVF with an interior crater and a gradual change in vegetation density between north- and south-facing hillslopes. (f) A cinder cone (34.19°N, 109.57°W) within the SVF, dated to 740–1110 kyr based on stratigraphy [*Hooper*, 1994], with vegetation restricted to channels on the north-facing side. (g) A cinder cone (41.64°N, 121.74°W) in the MLVF, dated to 180–300 kyr [*Donnelly-Nolan*, 2006].

4.3. Numerical Model

Colluvial and slope-wash/fluvial sediment transport processes can both contribute to the evolution of cinder cones, although colluvial transport processes are likely dominant on younger cones (which may lack overland flow entirely due to the highly porous nature of the initial cone prior to dust deposition). More broadly, *Perron et al.* [2008, 2009] have shown that hillslopes are dominated by colluvial processes; hence, cinder cones that lack substantial drainage development will almost certainly be dominated by colluvial processes. Colluvial transport is modeled as a transport-limited process with a sediment flux, q_s, that varies nonlinearly with hillslope gradient [*Roering et al.*, 1999]. Slope-wash/fluvial transport is modeled as a detachment-limited process, in which all eroded material is deposited outside of the model domain. Enforcing the conservation of mass allows for the rate of change of topography with time to be expressed as

$$\frac{\partial z}{\partial t} = -\nabla \cdot q_s - \epsilon, \tag{3}$$

where z is elevation, t is time, and ϵ is the slope-wash/fluvial detachment rate. The colluvial sediment flux is given by [*Roering et al.*, 1999]

$$q_s = -D\left(\frac{\nabla z}{1-(|\nabla z|/S_c)^2}\right), \tag{4}$$

where D is a colluvial transport coefficient that may vary in both space and time. Colluvial sediment flux increases nonlinearly as the hillslope gradient approaches a critical value, $S_c = 1.25$. Note that $\lim_{S_c \to +\infty} q_s = -D\nabla z$, which is the traditional, linear, slope-dependent transport law. The relationship between S_c, soil properties, vegetation, and critical angles for slope stability are not known but the chosen value of $S_c = 1.25$ is the same as that proposed by *Roering et al.* [1999] for their work in the Oregon Coast Range. In addition, the influence of slope-wash/fluvial processes on cone degradation can be seen through the formation of rills and gullies, which may eventually become organized into well-developed, semiperiodically spaced valleys [*Dohrenwend et al.*, 1986; *Hooper and Sheridan*, 1998] (Figure 5f). The slope-wash/fluvial detachment rate in the model has the general form [*Howard*, 1994; *Perron et al.*, 2008]

$$\epsilon = \begin{cases} K\left(A^p|\nabla z|^n - \theta_c\right) & A^p|\nabla z|^n > \theta_c \\ 0 & A^p|\nabla z|^n \le \theta_c \end{cases} \tag{5}$$

Here, K is an erodibility coefficient, A is the upstream contributing area, n and p are dimensionless constants, and θ_c is a critical entrainment threshold. We choose values of $p = 0.3$ and $n = 0.7$, which are associated with the commonly used shear stress erosion law [*Tucker and Whipple*, 2002].

Equation (3) is solved numerically using an explicit finite difference scheme. Let $z^c_{i,j}$ denote the value of z at the c^{th} computational time step and location $x = i\Delta x$ and $y = j\Delta y = j\Delta x$. Then define $D_{nl}(z) = D/(1 - (|\nabla z|/S_c)^2)$. The x and y components of the colluvial sediment flux are given by [*Perron*, 2011]

$$q^c_{i+1/2,j} = -\frac{1}{2}(D_{nl}(z_{i,j}) + D_{nl}(z_{i+1,j}))\left(\frac{z^c_{i+1,j} - z^c_{i,j}}{\Delta x}\right) \tag{6}$$

and

$$q^c_{i,j+1/2} = -\frac{1}{2}(D_{nl}(z_{i,j}) + D_{nl}(z_{i,j+1}))\left(\frac{z^c_{i,j+1} - z^c_{i,j}}{\Delta y}\right). \tag{7}$$

The value of $D_{nl}(z_{i,j})$ is approximated by

$$D_{nl}(z_{i,j}) = \frac{D_{i,j}}{1 - (z_x^2 + z_y^2)/S_c^2}, \tag{8}$$

where

$$z_x = \frac{z_{i+1,j} - z_{i-1,j}}{2\Delta x} \tag{9}$$

and

$$z_y = \frac{z_{i,j+1} - z_{i,j-1}}{2\Delta y}. \tag{10}$$

Defining S as the along-channel bed slope, the slope-wash/fluvial detachment rate can be written in discrete form as

$$\epsilon = \begin{cases} K_{i,j}\left(A^p_{i,j}S^n_{i,j} - \theta_c\right) & A^p_{i,j}S^n_{i,j} > \theta_c \\ 0 & A_{i,j}{}^pS^n_{i,j} \le \theta_c \end{cases} \tag{11}$$

We use the $D\infty$ flow routing method [*Tarboton*, 1997] to evaluate the upslope contributing area, $A_{i,j}$, and define $S_{i,j}$ as the maximum topographic gradient between the grid cell centered at $x = i\Delta x$ and $y = j\Delta y$ and the eight neighboring cells. Topographic elevation at the next time step is then determined by

$$z^{c+1}_{i,j} = z^c_{i,j} - \frac{\Delta t}{\Delta x}\left(q^c_{i+1/2,j} - q^c_{i-1/2,j}\right) - \frac{\Delta t}{\Delta y}\left(q^c_{i,j+1/2} - q^c_{i,j-1/2}\right) - \Delta t\epsilon. \tag{12}$$

Initially, cinder cones contain an interior crater, which poses a problem for flow routing algorithms such as $D\infty$ that do not realistically model flow over topography containing interior pits. Therefore, all pixels within the interior crater of the cinder cone do not contribute to A or to the slope-wash/fluvial erosion term within equation (3). The crater interior is small relative to the typical size of a cone, and at early times when it is the largest, slope-wash/fluvial erosion plays a relatively minor role in cinder cone degradation due to the porous nature of the surface. Interior pits may also form on other parts of the cone and are filled before applying the flow routing algorithm so that each pixel has a downslope neighbor [*Pelletier*, 2008].

The colluvial transport coefficient, D, can be estimated from landforms with known ages and can vary considerably with climate. *Hanks* [2000] reported values of D, consistent with the linear colluvial sediment flux law, of approximately 0.1–0.7 $m^2\ kyr^{-1}$ in arid regions of Israel, 0.5–2.0 $m^2\ kyr^{-1}$ in several semiarid to arid areas of the western U.S., and 11–16 $m^2\ kyr^{-1}$ in the more humid environments of coastal California and Michigan.

In section 5.2, we present estimates for the average value of D in the SFVF, SVF, and MLVF by comparing the temporal evolution of model-predicted cinder cones to the degradation observed on cinder cones with known age constraints. More specifically, we follow the methodology of *Hooper and Sheridan* [1998] and

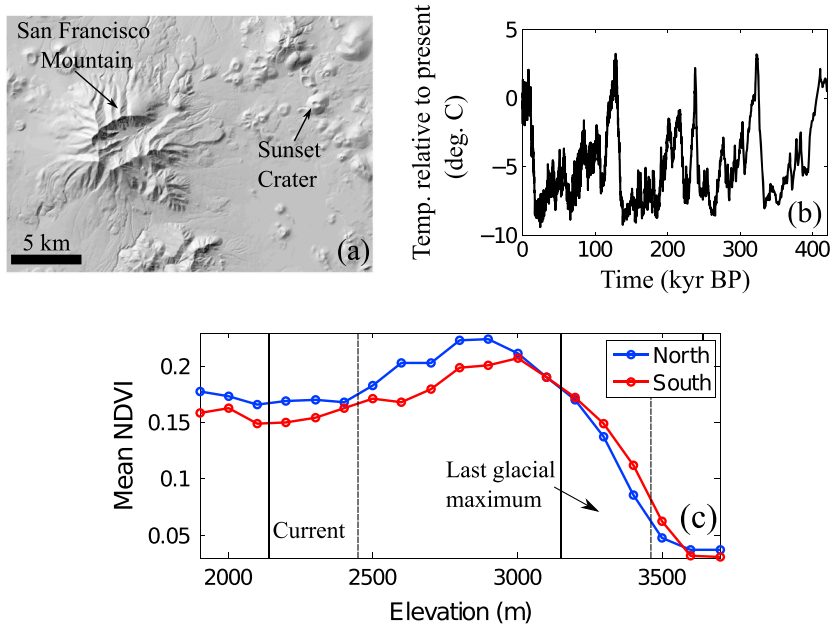

Figure 6. Trends in paleovegetation with northness can be estimated by using present-day vegetation statistics and temperature reconstruction data. (a) Hillshade of the region surrounding San Francisco Mountain in the SFVF within which NDVI was computed. (b) Atmospheric temperature relative to the mean present-day value, inferred from deuterium concentrations at Vostok, Antarctica [*Petit et al.*, 1999]. (c) Present-day NDVI for north- and south-facing hillslopes within the region of the SFVF contained in (a). During LGM, mean temperature was lower by $\approx$ 6°C, which corresponds to a shift in elevation of roughly 1000 m (assuming a lapse rate of 6°C km^{-1}). Vertical lines denote the mean elevation of cinder cones in the SFVF (solid) and SVF (dashed) as well as the mean "apparent elevation" of those same cinder cones during the last glacial maximum. South-facing slopes may have maintained higher biomass relative to north-facing slopes during the LGM.

compare numerical model predictions with statistical properties of cinder cones at various stages of development. Rates of colluvial transport were estimated within each study area by solving a one-dimensional version of equation (3), assuming spherical symmetry, the nonlinear colluvial sediment flux relationship, and $K = 0$ m$^{2/5}$ kyr^{-1}, and then comparing the temporal evolution of model-predicted cone slope to the actual decay in cone slope observed in that cone field. Mean cone slope decreases with time in the SFVF from approximately 26° for cones with an average age of $\approx$ 80 ka to 9° for cones with an average age of $\approx$ 3740 ka [*Hooper and Sheridan*, 1998]. A similar trend has been documented in the SVF, with the mean hillslope angle being approximately 16° on cones with a mean age of $\approx$ 635 ka and 9° on cones with a mean age of $\approx$ 1770 ka. A mean value of D was estimated for the SFVF and SVF by using cone morphology data compiled by *Hooper and Sheridan* [1998] since they calculated mean cone slope for a larger population of cones within these two fields. To estimate D in the MLVF, we compared model predictions with data presented herein for mean hillslope angle on cinder cones within five different age groups. Cones in the MVLF were placed within one of five age groups based on argon dates and stratigraphic relations compiled by *Donnelly-Nolan* [2006]. There are not a sufficient number of cones with well-constrained ages in the NVF to perform a similar calibration of D within that field.

We also use the numerical model in section 5.2 to test several different conceptual models that may explain asymmetries in hillslope gradient and drainage density on cinder cones by defining D and/or K as functions of northness. The value of $D(x, y)$ is based on a reference value, D_r, and a constant, D_v, that determines the variation in D associated with a northness difference of 1 (e.g., the difference between a south-facing hillslope with a gradient of 0.5 versus a north-facing hillslope with the same gradient). In particular, $D = D_r + \eta D_v$. Similarly, K varies linearly with northness around a reference value as $K = K_r + \eta K_v$. By comparing the morphology of model-predicted cinder cones to that of cinder cones in our study areas, we are able to assess the role of colluvial and slope-wash/fluvial processes in driving hillslope asymmetry in our study sites.

Hooper and Sheridan [1998] averaged data from 70 recently emplaced cinder cones (< 160 ka) to approximate the typical form of a young cone. We use these same parameters to define an initial condition for

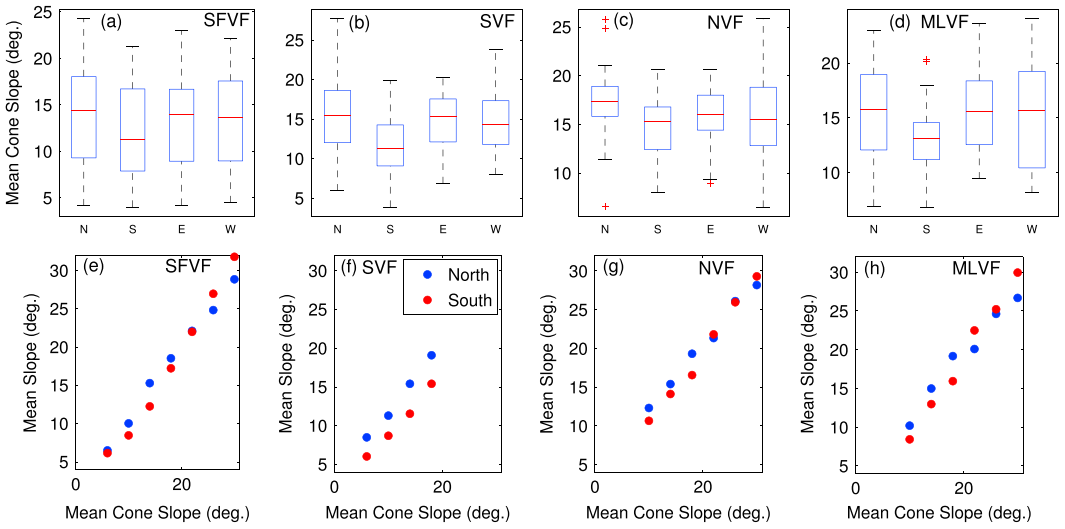

Figure 7. Hillslope angle on north, south, east, and west-facing sides of cinder cones. Boxplots of mean hillslope angle computed in each of the four cardinal directions on older cinder cones (mean hillslope angle less than 20°) within the (a) SFVF, (b) SVF, (c) NVF, and (d) MLVF. Mean hillslope angle on north- and south-facing hillslopes on cinder cones as a function of mean cone slope for the (e) SFVF, (f) SVF, (g) NVF, and (h) MLVF. Cinder cones evolve asymmetrically with north-facing hillslopes becoming steeper than south-facing hillslopes over time.

numerical simulations. The initial condition used for all simulations is a cone with a topographic slope of 30°, a basal diameter of 876 m, and an interior crater with diameter 292 m. All numerical simulations are performed on a square mesh with a grid spacing of 4 m unless noted otherwise. Neumann boundary conditions are imposed at the edges of the computational domain.

5. Results

5.1. Statistical Analyses of Topography, Vegetation Patterns, and Drainage Density

NDVI increases with northness in each of the four volcanic fields (Figure 5). The largest difference in NDVI between north- ($\eta > 0$) and south-facing ($\eta < 0$) hillslopes is found in the *NVF*, while the smallest difference occurs in the *SVF*. The relationship between northness and NDVI, however, varies with elevation (Figure 6). At relatively low elevations in the SFVF where cinder cones are located (i.e., 1600–2700 m a.m.s.l.), NDVI is

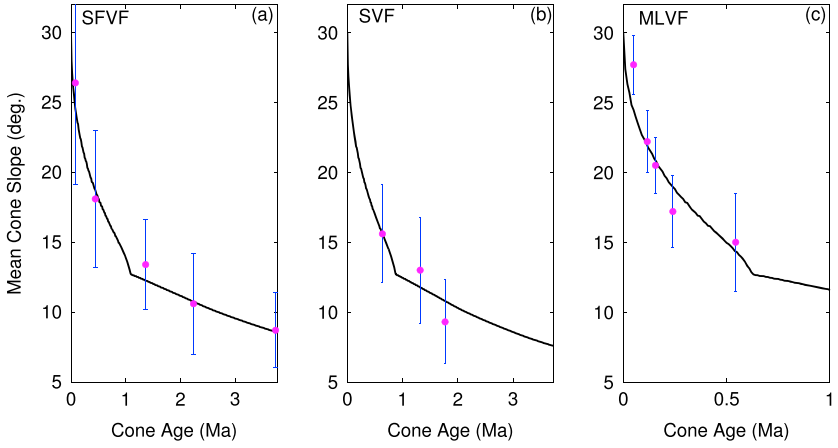

Figure 8. Comparison between model-predicted cinder cone evolution and data compiled for the SFVF, SVF, and MLVF. We use a 1d, spherically symmetric model with $\Delta x = 2.5$ m and neglect slope-wash/fluvial transport. Model-predicted mean cone slope is shown as a function of time for a cinder cone (black line) in the (a) SFVF, (b) SVF, and (c) MLVF. The mean slope of cinder cones with known age constraints are shown (solid dots) for comparison along with error bars (±1 standard deviation). Colluvial transport coefficients of 4.0 $m^2\ kyr^{-1}$, 5.0 $m^2\ kyr^{-1}$, and 7.5 $m^2\ kyr^{-1}$ are found to be most consistent with the data in the SFVF, SVF, and MLVF respectively.

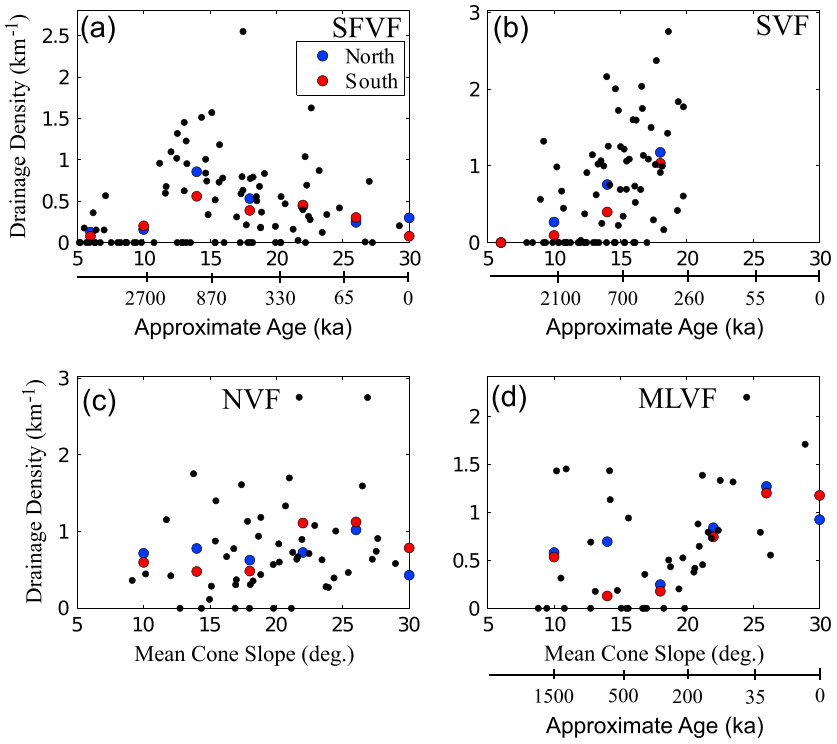

Figure 9. Drainage density as a function of mean cinder cone slope, a proxy for cone age. Approximate age (ka), estimated using the numerical model, is shown for the SFVF, SVF, and MLVF, where we were able to estimate *D*. Blue and red dots represent average drainage density within 4° intervals on north- and south-facing hillslopes. Drainage density in the (a) SFVF and (c) NVF is low when the mean cone slope angle is high but then increases slowly with decreasing cone slope (increasing age) before decreasing again on highly degraded cones. (b) In the SVF, drainage density is highest on cones with intermediate hillslope angles and decreases with decreasing cone slope (increasing age). (d) Drainage density in the MLVF is low relative to that found in the other three volcanic fields and does not appear to vary with mean cone slope.

consistently higher on north-facing hillslopes. At elevations in the range of 3200–3500 m, however, this relationship is reversed; that is, NDVI on south-facing hillslopes is greater than that on north-facing hillslopes. As such, we conclude that NDVI (i.e., a proxy for vegetation density) is greater today on the north-facing hillslopes of most cinder cones within the SFVF, but it was greater on south-facing hillslopes in an environment that is wetter and approximately $5-9$°C cooler, that is, similar to the conditions that prevailed during most of the Pleistocene (Figure 6).

Plotting mean hillslope angle on the north- and south-facing sides of cinder cones as a function of mean cone slope suggests that hillslope asymmetry becomes apparent on cones with mean hillslope angles less than approximately 20° (Figure 7). We used the numerical model to quantify the relationship between mean cone slope and cone age within three of the volcanic fields (Figure 8). A mean cone slope of 20° corresponds to an age of approximately 200 ka, 260 ka, and 330 ka in the MLVF, SVF, and SFVF, respectively. Drainage networks develop slowest on cones within the SFVF, the driest study site, but nonetheless have begun to develop on cones within each of the study areas by the time that they erode to have a mean hillslope angle of ≈15–20° (330–870 kyr) (Figure 9).

First, we use statistical testing to determine if hillslope asymmetry exists on young cinder cones, that is, those with mean topographic slopes greater than 20°. A *t* test, with a significance level of $\alpha = 0.05$, was used to test the null hypothesis that there is no difference in mean between the distributions of measured hillslope angles. The results of the significance tests and the number of cinder cones analyzed in each study area are summarized in (Table 1). Mean hillslope angles on north- and south-facing hillslopes are found to be statistically similar in populations of young cones with the exception of north- and south-facing hillslopes in the MLVF ($p \approx 0.04$), where south-facing hillslope angles are higher. Note that there are no young cones within the SVF since none of the selected cinder cones has a mean hillslope angle greater than 20°.

Table 1. Average Hillslope Angle, Shown as Mean Plus/Minus Standard Deviation, for North- and South-Facing Hillslopes of Young Cinder Cones (S_{ny} and S_{sy}, Respectively) and Old Cones (S_{no} and S_{so}, Respectively) in the Four Study Areas[a]

Field Name	n_y	S_{ny} (deg)	S_{sy} (deg)	t test	n_o	S_{no} (deg)	S_{so} (deg)	t test
SFVF	20	21.8 ± 4.0	22.5 ± 5.0	0 (0.56)	73	14.2 ± 5.6	12.4 ± 5.2	1 (< 0.01)
SVF	0	–	–	–	80	15.4 ± 4.3	11.9 ± 3.6	1 (< 0.01)
NVF	24	23.2 ± 3.3	23.5 ± 3.4	0 (0.69)	26	17.3 ± 4.0	15.1 ± 3.0	1 (0.02)
MLVF	16	21.8 ± 3.3	23.9 ± 3.8	1 (0.04)	26	15.5 ± 4.3	13.1 ± 3.6	1 (< 0.01)

[a]Statistics are computed from a population of n_y young cones and n_o old cones in each field. A t test ($\alpha = 0.05$) is used to determine if the means of the north- and south-facing hillslope angle distributions are different. A value of 0 indicates that the null hypothesis (means are equal) cannot be rejected, while a value of 1 indicates that the null hypothesis can be rejected. The p-value from the test is shown in parentheses.

Similarly, the t test ($\alpha = 0.05$) was used to test the null hypothesis that there is no difference in mean between the distributions of measured north- and south-facing hillslope angles on older cones. Mean hillslope angle on the north-facing side of cinder cones is higher than that on south-facing hillslopes and the null hypothesis is rejected in all four volcanic fields (Table 1). There is no statistical difference in the mean hillslope angle between populations of east- and west-facing hillslopes on young cones or older cones with the single exception of east and west-facing hillslopes on young cones in the SFVF ($p \approx 0.02$).

In addition, asymmetries in maximum hillslope angle (as measured over a distance of 30 m along transects) between north- and south-facing hillslopes are assessed similarly. Maximum hillslope angles along north-facing transects on older cones within the SFVF, SVF, NVF, and MLVF are 22.2°, 23.2°, 25.1°, and 23.1°, respectively. Maximum hillslope angles along south-facing transects are 18.6°, 17.4°, 22.2°, and 18.2°, respectively. For young cones, we determine that the null hypothesis (i.e., that the maximum value of north- and south-facing hillslope angles are equal) cannot be rejected in any of the four volcanic fields. The null hypothesis is rejected for north- and south-facing hillslopes on older cones in all volcanic fields. There is no difference in the mean of east- and west-facing maximum hillslope angle on young or old cones with the exceptions of young cones in the SFVF ($p \approx 0.02$) and old cones in the SVF ($p < 0.01$).

Error analyses performed through comparison of NED-derived DEMs and lidar-derived DEMs show that differences in hillslope angle computed between the two sets of DEMs are minor ($< 1°$) relative to the reported asymmetries in hillslope angle, which are $2° - 4°$ on average. Less than 5% of all hillslope angle measurements (including measurements along individual transects) differ by more than 10%.

Next, we use statistical testing to determine if differences in drainage density between north- and south-facing hillslopes are significant on populations of young and old cinder cones. Only cinder cones that have a drainage density greater than zero are included in the significance testing. Since channel development is a threshold-dependent process, the same differences in sediment transport processes may exist on cones with and without drainage development, but these process variations are undetectable if critical thresholds for channel development are not met. In other words, cinder cones that have a drainage

Table 2. Mean Drainage Density (± 1 Standard Deviation) on the North- and South-Facing Hillslopes of Young (DD_{ny} and DD_{sy}, Respectively) and Old (DD_{no} and DD_{so}, Respectively) Cinder Cones in the San Francisco Volcanic Field, Springerville Volcanic Field, Newberry Volcanic Field, and Medicine Lake Volcanic Field[a]

Field Name	n_y	DD_{ny} (km^{-1})	DD_{sy} (km^{-1})	U test	n_o	DD_{no} (km^{-1})	DD_{so} (km^{-1})	U test
SFVF	14	0.49 ± 0.63	0.50 ± 0.56	0 (0.77)	41	0.87 ± 0.63	0.62 ± 0.52	1 (0.04)
SVF	0	–	–	–	49	1.22 ± 0.73	0.82 ± 0.79	1 (< 0.01)
NVF	23	0.84 ± 0.69	1.15 ± 1.06	0 (0.50)	21	0.85 ± 0.65	0.61 ± 0.46	0 (0.30)
MLVF	16	0.93 ± 0.75	0.88 ± 0.67	0 (0.90)	14	0.92 ± 0.76	0.45 ± 0.64	1 (0.05)

[a]Cinder cones are only included in drainage density statistics if the mean cone drainage density is greater than zero. Statistics are computed from populations of n_o old cones and n_y young cones in each field. A Mann-Whitney U test is used to determine if there is a significant difference in median drainage density between north- and south-facing sides of the cones. A value of 0 indicates that the null hypothesis (medians are equal) cannot be rejected at the standard $\alpha = 0.05$ level, while a value of 1 indicates that the null hypothesis can be rejected. The p-value from the test is shown in parentheses.

Table 3. Mean Cone Slope (±1 Standard Deviation) Within Five Different Age Groups of Cinder Cones in the MLVF[a]

Cone Age (kyr)	*n*	Mean slope (deg)
0–100	4	27.7 ± 2.1
100–132	8	22.2 ± 2.2
132–180	10	20.5 ± 2.0
180–300	4	17.2 ± 2.6
300–788	4	15.0 ± 3.5

[a]The number of cones within each age group is denoted by *n*.

density of zero on both north- and south-facing hillslopes do not provide significant information about the presence/absence of slope-aspect-driven variations in the processes influencing drainage density.

The distributions of drainage density on north- and south-facing hillslopes within the four study sites are highly skewed, partly due to the frequency of cinder cones that may have no significant drainage development on one side of the cone. Therefore, a Mann-Whitney *U* test ($\alpha = 0.05$) is used to test the null hypothesis that there is no difference in median between the distributions of measured drainage density on north- and south-facing hillslopes. Differences in drainage density on young cones are not statistically significant in any of the study areas. On older cones, drainage density is higher on the north-facing hillslopes in all four study areas, but the median drainage densities on north- and south-facing hillslopes are only found to be statistically different within the SFVF, SVF, and MLVF. Mean drainage densities for north- and south-facing hillslopes, the number of cones included in the analysis, and the results of the significance tests are presented in Table 2.

By examining patterns in drainage density as a function of mean cone slope, we are also able to study the evolution of drainage development on cinder cones as a function of time. When the mean cone slope angle is high, indicative of relatively young cones, there is little drainage development (Figure 9). In the SFVF and NVF, drainage density increases initially with decreasing mean cone slope (increasing age). Following this peak, drainage density begins to decrease with decreasing mean cone slope (increasing age). There are no young cones within the SVF, but drainage density does decrease on older cones in a manner that is consistent with the pattern observed in the SFVF and NVF. Average drainage density is highest in

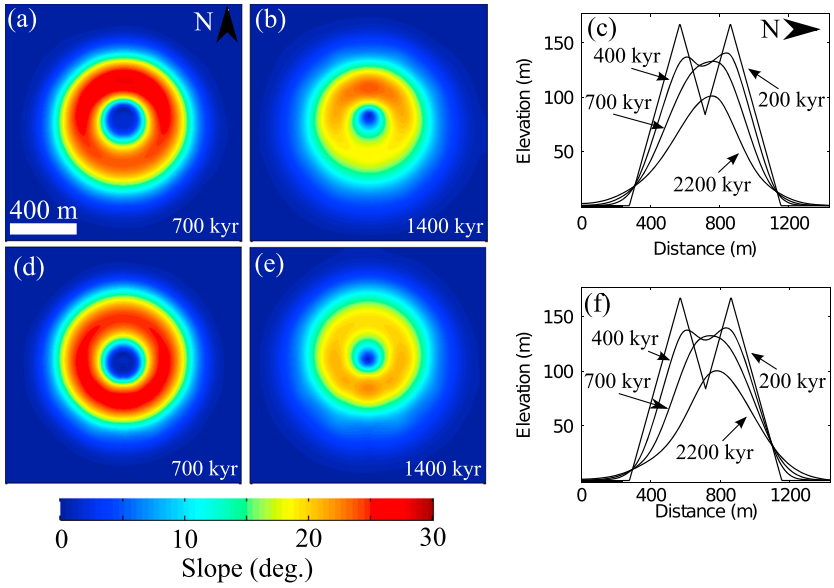

Figure 10. Topographic slope and topographic cross sections of model-predicted cinder cones at selected time intervals. A spatially variable colluvial transport rate, defined by $D_r = 5$ m^2 kyr^{-1} and $D_v = -1.5$ m^2 kyr^{-1}, results in topographic asymmetries that are similar in magnitude to those observed in the four study areas. (a) At $t = 700$ kyr, the interior crater has been filled and north-facing hillslopes are steeper than south-facing hillslopes. (b) At $t = 1400$ kyr, asymmetries in hillslope angle are more apparent. (c) South-north cross sections of topography show that initial cone slope is 30°, but after 400 kyr there is a noticeable difference between the mean angle on north- and south-facing hillslopes. Other parameters used in Figures 10a–10c are $K_r = 0.0125$ m$^{2/5}$ kyr^{-1}, $K_v = 0$ m$^{2/5}$ kyr^{-1}, and $\theta_c = 1.5$. (d–f) A spatially variable erodibility coefficient, defined by $K_r = 0.0125$ m$^{2/5}$ kyr^{-1} and $K_v = -0.0094$ m$^{2/5}$ kyr^{-1}, also results in hillslope asymmetry. (d) At $t = 700$ kyr and (e) $t = 1400$, the mean hillslope angle is greatest on the north-facing side, but the highest local topographic slope values are found on the south-facing side. (f) Topography along south-north cross sections. Other parameters used in Figures 10d–10f are $D_r = 5$ m^2 kyr^{-1}, $D_v = 0$ m^2 kyr^{-1}, and $\theta_c = 1.5$.

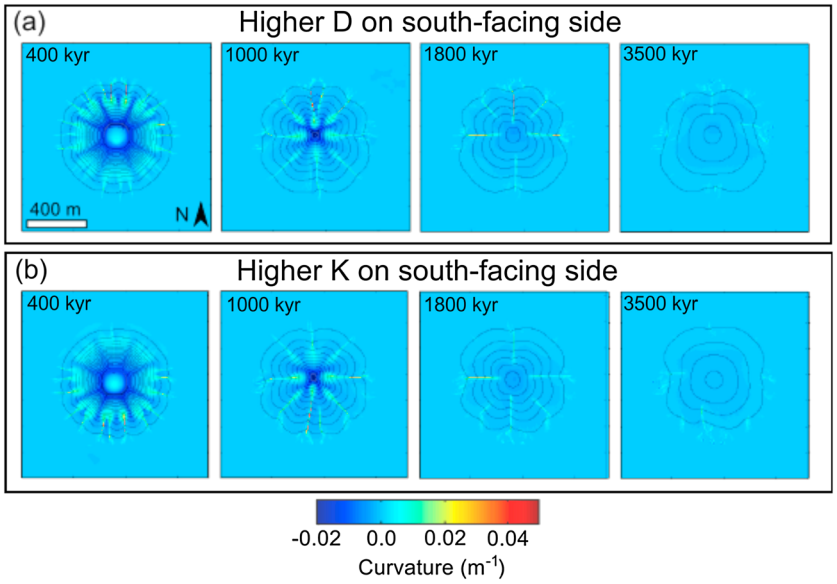

Figure 11. Contour plots are shown over maps of topographic curvature for a model-predicted cinder cone degrading with a (a) spatially variable colluvial transport coefficient that decreases with increasing northness and constant erodibility coefficient as well as a (b) spatially variable erodibility coefficient that decreases with northness and a constant colluvial transport coefficient. The contour interval is 8 m. Drainage density is controlled by the importance of colluvial sediment transport relative to slope-wash/fluvial sediment transport. Parameters used in Figure 11a are $K = 0.0625\ m^{2/5}\ kyr^{-1}$, $K_v = 0\ m^{2/5}\ kyr^{-1}$, $\theta_c = 1.5$, $D_v = -1.5\ m^2\ kyr^{-1}$, $D = 5\ m^2\ kyr^{-1}$. Parameters used in Figure 11b are $K = 0.0625\ m^{2/5}\ kyr^{-1}$, $K_v = -0.0312\ m^{2/5}\ kyr^{-1}$, $\theta_c = 1.5$, $D_v = 0\ m^2\ kyr^{-1}$, $D = 5\ m^2\ kyr^{-1}$.

the NVF and lowest in the MLVF. Error analyses performed through comparison of NED-derived DEMs and lidar-derived DEMs shows that differences in computed drainage density between the two sets of DEMs are small ($\approx 0.2\ km^{-1}$) relative to the reported variations in drainage density with cone age (Figure 9).

5.2. Numerical Modeling

Following *Hooper and Sheridan* [1998], we estimate rates of colluvial sediment transport in the SFVF, SVF, and MLVF by comparing numerical model predictions with statistical properties of cinder cones at different stages of development. *Hooper and Sheridan* [1998] demonstrated, using statistics obtained from a large population of cinder cones, that mean cone slope decreases with age in the SFVF and SVF (Figure 8). The results of our analysis of the relationship between mean cone slope and cone age in the MLVF are summarized in Table 3. Model predictions show that a value of $D = 4.0\ m^2\ kyr^{-1}$ is the most consistent with data for the SFVF while higher values of $D = 5.0\ m^2\ kyr^{-1}$ and $D = 7.5\ m^2\ kyr^{-1}$ result in the best agreement with data for the SVF and MLVF, respectively (Figure 8).

Lower hillslope angles and lower drainage densities are observed on south-facing hillslopes relative to north-facing hillslopes within all four study areas. These asymmetries likely result from spatial variations in the rates of slope-wash/fluvial and/or colluvial sediment transport processes. Using the numerical model, we test several different scenarios in which D and K vary with northness in order to isolate the relationship(s) between D, K, and northness that produce(s) cinder cone morphologies consistent with observations. Model predictions that result in cinder cones having greater (mean and maximum) topographic slopes and higher drainage density on the north-facing side of the cone relative to the south-facing side are considered to be consistent with the observations from our study areas. Both D and K are chosen to vary with northness since it is likely that vegetation has varied with northness in our study areas under present and previous climatic conditions (Figures 5 and 6). In all cases, we choose a reference value of $D_r = 5\ m^2\ kyr^{-1}$ since this is the estimated value for the SVF and it is in this field site that we document the most significant differences in hillslope morphology (i.e., topographic slope and drainage density) between north- and south-facing hillslopes.

First, we test the idea that asymmetries in hillslope angle and drainage density can occur primarily as a result of increased colluvial transport on south-facing hillslopes relative to north-facing hillslopes by assuming $K_v = 0\ m^{2/5}\ kyr^{-1}$ (K is independent of northness) and $D_v = -1.5\ m^2\ kyr^{-1}$ (D decreases with northness).

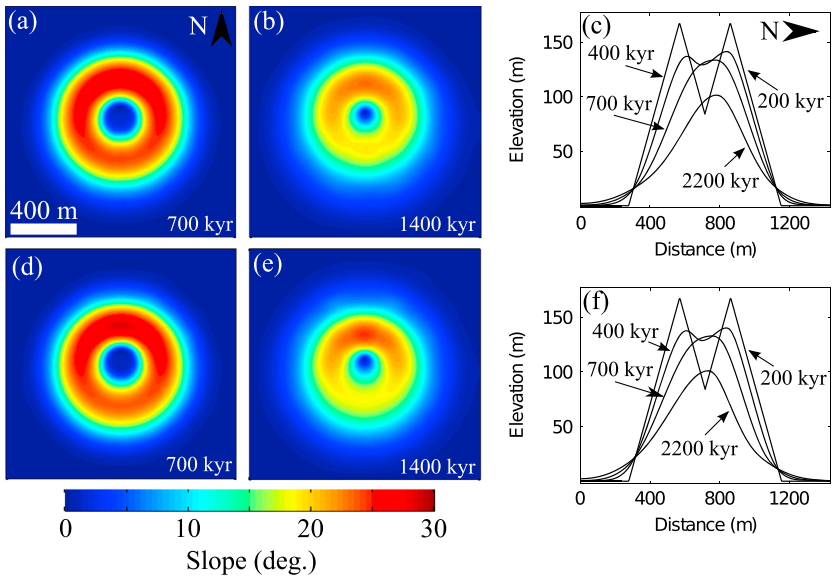

Figure 12. Topographic slope and topographic cross sections of model-predicted cinder cones at selected time intervals. Hillslope asymmetry results from D and K both being decreasing functions of northness. (a–b) At both $t = 700$ kyr and 1400 kyr, north-facing hillslopes appear steeper than south-facing hillslopes. (c) South-north cross sections of topography show that initial cone slope is 30°, but after 400 kyr there is a noticeable difference between the mean angle on north- and south-facing hillslopes. Parameters used in Figure 12a are $K_r = 0.0125$ m$^{2/5}$ kyr^{-1}, $K_v = -0.0037$ m$^{2/5}$ kyr^{-1}, $\theta_c = 1.5$, $D_r = 5$ m^2 kyr^{-1}, and $D_v = -1.5$ m^2 kyr^{-1}. (d-f) Higher mean and maximum hillslope angles on the north-facing side of the cone can also be the result of D decreasing with northness and K increasing with northness. Parameters used in Figures 12d–12f are $K_r = 0.0125$ m$^{2/5}$ kyr^{-1}, $K_v = 0.0037$ m$^{2/5}$ kyr^{-1}, $\theta_c = 1.5$, $D_r = 5$ m^2 kyr^{-1}, and $D_v = -1.5$ m^2 kyr^{-1}.

A larger colluvial transport coefficient on south-facing hillslopes could be associated with increased vegetation cover, which our paleovegetation analysis suggests was the case during the glacial climates that dominated the Pleistocene, and/or more frequent freeze-thaw cycles. Numerical-model predictions demonstrate, in this case, that the mean angle of north-facing hillslopes will evolve to be several degrees higher than south-facing hillslopes (Figure 10c). After 400 kyr, the mean hillslope angles on north- and south-facing sides of the cone are 20° and 17°, respectively while they are 10° and 8°, respectively, after 2200 kyr. Maximum hillslope angles on the north-facing side of the cone, approximately 29° after 400 kyr and 19° after 2200 kyr, are higher than the highest hillslope angles found on the south-facing side, roughly 25° after 400 kyr and 15° after 2200 kyr (Figure 10b). Additionally, drainage density is greater on north-facing hillslopes in cases where K_r is high enough to promote significant drainage development (Figure 11a). Under these conditions, model predictions show the formation of a large number of small gullies, developing preferentially on the north-facing hillslope, after several hundred thousand years. Rounding of the crater rim occurs more slowly on the north-facing side of the cone (Figure 11). After $t = 400$ kyr, north- and south-facing sides of the cone have mean hillslope angles of approximately 20° and 17°, respectively, and maximum hillslope angles of 34° and 30°, respectively. At approximately 1000 kyr, incised valleys have formed and the interior crater is completely filled. By 1800 kyr, some previously developed valleys have filled and others are beginning to fill. After $t = 2200$ kyr, mean hillslope angles are 6° and 5° on the north- and south-facing sides of the cone and maximum hillslope angles are 10° and 7° for north- and south-facing sides, respectively. Boundaries of the cinder cone are poorly defined and there are no identifiable channels remaining after 3500 kyr (Figure 11). Model predictions of cone morphology with a hypothetically larger value of D on south-facing hillslopes are consistent with observations from the four study areas. From these model predictions and the symmetry of this problem, it is also possible to infer the result of defining D as an increasing function of northness. An increase in D on north-facing hillslopes (i.e., $D_v > 0$) would result in cinder cones having gentler north-facing hillslopes and higher drainage density on south-facing hillslopes, which would be inconsistent with observations.

We also test the conceptual model that steeper hillslope angles and higher drainage density on north-facing hillslopes occur as the result of spatial variations in the slope-wash/fluvial erodibility coefficient, K, by

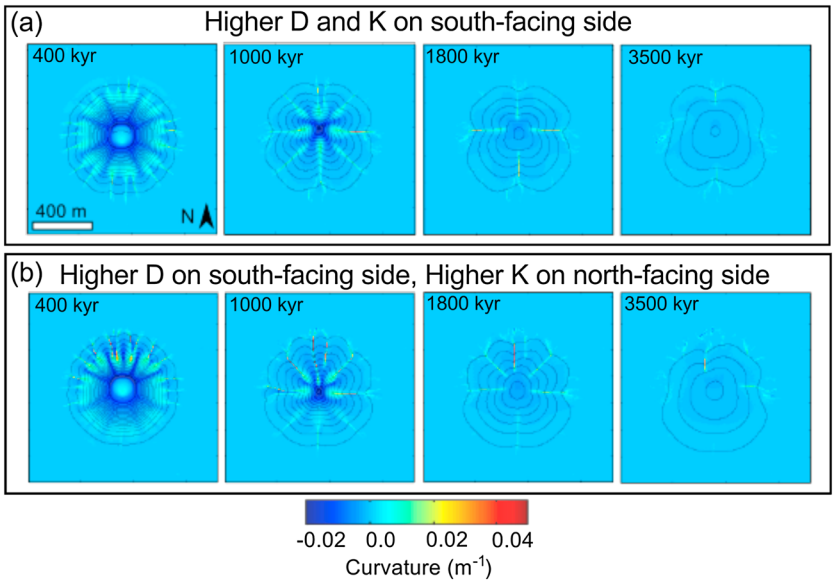

Figure 13. Contour plots are shown over maps of topographic curvature for a model-predicted cinder cone degrading with a (a) spatially variable colluvial transport coefficient, D, and erodibility coefficient, K, that both decrease with northness as well as a (b) spatially variable erodibility coefficient that increases northness and a colluvial transport coefficient that decreases with northness. The contour interval is 8 m. Drainage density is controlled by the importance of colluvial sediment transport relative to slope-wash/fluvial sediment transport. Parameters used in Figure 13a are $K_r = 0.0625\ m^{2/5}\ kyr^{-1}$, $K_v = -0.0187\ m^{2/5}\ kyr^{-1}$, $\theta_c = 1.5$, $D_v = -1.5\ m^2\ kyr^{-1}$, $D_r = 5\ m^2\ kyr^{-1}$. Parameters used in (b) are $K = 0.0625\ m^{2/5}\ kyr^{-1}$, $K_v = 0.0187\ m^{2/5}\ kyr^{-1}$, $\theta_c = 1.5$, $D_r = 5\ m^2\ kyr^{-1}$, and $D_v = -1.5\ m^2\ kyr^{-1}$.

defining $K_r = 0.0125\ m^{2/5}\ kyr^{-1}$, $K_v = -0.0094\ m^{2/5}\ kyr^{-1}$, and $D_v = 0\ m^2\ kyr^{-1}$. In this case, D is constant and K is greater on south-facing hillslopes. Increases in K on south-facing hillslopes could be associated with less vegetation cover, which is observed under present-day conditions (Figure 5) but may not have existed throughout much of the Quaternary (Figure 6). A higher erodibility coefficient on the south-facing side of the cone leads to faster degradation of the south-facing crater rim and shifts the center of the cone slightly with time. After 400 kyr and 2200 kyr, north-facing sides of the cone have mean hillslopes angles of 19° and 10°, respectively, while mean hillslope angles on the south-facing side are 19° and 9° respectively (Figure 10f). The steepest sections of south-facing hillslopes are consistently steeper than the steepest sections of north-facing hillslopes (Figure 10e). These differences in hillslope angle between north- and south-facing sides of the cone are minor because values of K must be kept small to prevent channel development. If K_r is high enough to promote significant channel development, then drainage density is greater on south-facing hillslopes (Figure 11b). Model predictions of cinder cone morphology with a hypothetically larger K value on south-facing hillslopes are therefore inconsistent with observations. Likewise, it follows that defining K as an increasing function of northness (i.e., $K_v > 0$) would result in model-predicted cinder cones having north-facing hillslopes with lower (or similar) mean topographic slopes relative to south-facing hillslopes, which is not consistent with the documented hillslopes asymmetry in our study areas.

The coefficients D and K may also covary. When $D_v = -1.5\ m^2\ kyr^{-1}$, $K_r = 0.0125\ m^{2/5}\ kyr^{-1}$, and $K_v = -0.0037\ m^{2/5}\ kyr^{-1}$ so that D and K are both decreasing functions of northness, mean and maximum hillslope angles on the south-facing side of the cone are lower than those on the north-facing side (Figure 12). After 400 kyr and 2200 kyr, mean hillslope angles on the north-facing side of the cone are 20° and 11°, respectively, while they are 18° and 9° on the south-facing side. If significant channel development occurs, drainage density is similar on both sides of the modeled cone (Figure 13a). Since drainage density is observed to be higher on the north-facing side of cinder cones in our study areas, the hypothetical situation that both D and K are greater on south-facing hillslopes is inconsistent with observations. We do not directly test the case where D and K are both greater on north-facing hillslopes. It can be inferred, however, from the last case that such a scenario would result in north-facing hillslopes having lower topographic slopes, which is also inconsistent with observations.

Defining D as a decreasing function of northness ($D_v = -1.5$ m^2 kyr^{-1}) and K as an increasing function of northness ($K_r = 0.0125$ m$^{2/5}$ kyr^{-1}, $K_v = 0.0037$ m$^{2/5}$ kyr^{-1}) can also result in mean and maximum hillslope angles that are lower on the south-facing side of the cone (Figure 12). After 400 and 2200 kyr, mean hillslope angles on the north-facing side of the cone are 20° and 11°, respectively, while they are 18° and 9° on the south-facing side. Further, if K is defined using $K_r = 0.0625$ m$^{2/5}$ kyr^{-1} and $K_v = 0.0187$ m$^{2/5}$ kyr^{-1}, channel development occurs and drainage density is greater on the north-facing side of the cone (Figure 13b). In this case, mean hillslope angles on the north-facing side of the cone are 19° and 6° after 400 kyr and 2200 kyr, respectively, while they are 17° and 5° on the south-facing side after 400 kyr and 2200 kyr. Maximum hillslope angles on the north-facing side of the cone are approximately 34° and 8° after 400 kyr and 2200 kyr, respectively, while they are roughly 29° and 7° on the south-facing side after 400 kyr and 2200 kyr. These model predictions, with D being greater on south-facing hillslopes and K being greater on north-facing hillslopes, are consistent with observations. It is not necessary to test the case where D and K are higher on north- and south-facing hillslopes, respectively, because the result can again be inferred directly from the previous case. Therefore, a hypothetically larger K value on south-facing hillslopes and larger D value on north-facing hillslopes would result in higher drainage density on the south-facing side of the cone if channel development occurs and would be inconsistent with observations. Additionally, based on these results we expect a larger K value on south-facing hillslopes and larger a D value on north-facing hillslopes to lead to gentler north-facing hillslopes, which would also be inconsistent with observations.

6. Discussion

6.1. Asymmetries in Hillslope Angle

Our data suggest that slope-aspect-driven microclimatic effects have influenced the geomorphic evolution of cinder cones within the SFVF, SVF, NVF, and MLVF. Mean and maximum hillslope angles are both found to be higher on north-facing hillslopes compared to south-facing hillslopes within populations of older cones in each volcanic field. There is no statistically significant difference between the mean hillslope angle of east- and west-facing hillslopes on older cinder cones within any of the volcanic fields. Further, hillslope angles on east and west-facing hillslopes tend to be intermediate to those on corresponding north- and south-facing hillslopes (Figure 7). Both mean and maximum hillslope angles on north and south as well as east- and west-facing hillslopes are found to be statistically similar in populations of young cones with only a few exceptions.

Wind transport of tephra during a volcanic eruption can produce initially asymmetric cinder cones. However, we found that north-facing hillslopes are consistently steeper than south-facing hillslopes on cones with mean hillslope angles of $\approx$ 20°, $\approx$ 15°, and $<$ 10° (Figure 7). The consistency of this trend within all four volcanic fields on older cones with a range of ages suggests that it is unlikely that cinder cone eruption processes are responsible for hillslope asymmetry on those cones. The relative lack of hillslope asymmetry found on younger cones also lends support to this hypothesis.

Hillslope asymmetry is statistically significant in all four volcanic fields on cinder cones with a mean hillslope angle below $\approx$ 20° (Figure 7). If slope-aspect-induced variations in sediment transport processes are responsible for the asymmetry, sufficient time must pass before such variations result in observable differences between north- and south-facing hillslopes. It takes approximately 200 kyr in the MLVF for a cinder cone to degrade to the point where its mean hillslope angle is 20°, whereas 260 kyr and 330 kyr are needed in the SVF and SFVF, respectively. However, it is not unexpected that the time required to develop hillslope asymmetry on cinder cones varies with climate, and the distance to aeolian dust sources since the time required for soil and vegetation development also depends on these factors. Mineralogical differences may also contribute to variations in the time required for the development of hillslope asymmetry. Many of the mechanisms likely to drive the development of hillslope asymmetry, for example, bioturbation and freeze-thaw cycles, require the development of a soil capable of retaining moisture and supporting vegetation. The chosen threshold hillslope angle of 20° should be thought of as a rough approximation of the time needed for these processes to become active and result in hillslope asymmetry on cinder cones in our study areas.

Lower hillslope angles on the south-facing sides of cinder cones in our four study sites indicate relatively high rates of geomorphic degradation of those hillslopes compared with north-facing hillslopes. The observation that hillslope asymmetry appears predominantly between north- and south-facing hillslopes rather than east and west-facing hillslopes is consistent with the interpretation that microclimatic differences,

which are maximized between north- and south-facing hillslopes, are responsible for generating the mechanisms that result in the asymmetries. It is noteworthy that north-facing hillslope angles are consistently steeper than south-facing hillslope angles within all four study areas despite differences in present-day regional climate ($PE = 45$ (in/°F)$^{10/9}$ in SVF and $PE = 110$ (in/°F)$^{10/9}$ in MLVF) and vegetation type among the different volcanic fields.

6.2. Drainage Development on Cinder Cones

Drainage density is low in all cases relative to previously published studies [e.g., *Melton*, 1957; *Howard*, 1997], but this may be attributed to the initially porous nature of cinder cones. More generally, drainage density appears to increase with age, up to a point, in the SFVF and NVF, after which it decreases with age due to relief reduction. These results are qualitatively similar to those of *Howard* [1997] in that areas of low relief (e.g., old, degraded cones) are associated with low drainage density as are areas of high relief (e.g., newly emplaced cones). *Howard* [1997], in his study of badlands topography in Utah, documented a dependence of drainage density on the relief ratio, a measure of relief normalized by hillslope length. Howard's study suggests that strong feedbacks exist among drainage development, erosion rates, and topography. In our study areas, the initial increase in drainage density as cones degrade suggests that slope-wash/fluvial erosion is limited at first by a lack of runoff (Figure 9). Particularly in drier environments, runoff is limited on young cinder cones by the rapid infiltration of water through the porous cinders at the cone surface. Once dust accumulation or weathering-based soil production decreases the infiltration rate near the cone surface, runoff can be generated and drainage density increases. After cones have aged and developed soil, infiltration rates may be lower but runoff may not generate sufficient shear stress to continue to maintain previously developed channels because hillslope angles are lower on older, more degraded cones.

In addition to examining the temporal development of channels on cinder cones, we computed the drainage density on north- and south-facing hillslopes of cinder cones in all four volcanic fields to determine if variations in vegetation, driven by microclimate, lead to differences in drainage density. The north-facing hillslopes of older cinder cones have higher drainage densities than south-facing hillslopes in all four study areas, with differences in the median drainage density being statistically significant in the SFVF, SVF, and MLVF. These results lend support to the hypothesis that drainage density is influenced by slope aspect within our study areas. There is a relatively small sample size of older cones in the MLVF, however, and only a small number of cones show evidence of channel development (12 of the 26 old cones have zero drainage density). Therefore, even though differences in drainage density are significant at the $\alpha = 0.05$ level in the MLVF, we interpret these results with caution.

6.3. Interactions Among Climate, Vegetation, and Hillslope Morphology

The colluvial transport coefficient, D, is thought to vary with climate [e.g., *Hanks*, 2000] but, in general, is a poorly constrained parameter in many landscape evolution models. Three of the four study areas have a sufficient number of dated cinder cones to allow for estimates of D averaged over the life of a cone (Figure 8). We find best fit values of $D = 4.0$ m^2 kyr^{-1}, $D = 5.0$ m^2 kyr^{-1}, and $D = 7.5$ m^2 kyr^{-1} in the SFVF, SVF, and MLVF, respectively.

Results suggest that the simple landscape evolution model described here is capable of reproducing the asymmetries in cinder cone degradation that develop over time. Using the numerical model, we explored the relationship between cinder cone morphology and spatial variations in D and K in cases with and without significant drainage development. From the hypothetical scenarios tested, those characterized by a higher value of D on south-facing hillslopes produce cinder cones with landscape characteristics that are most consistent with observations (i.e., north-facing hillslopes are steeper and have greater drainage density if channels develop), whereas those characterized by higher or equal values of D on north-facing hillslopes fail to reproduce the asymmetries observed on cinder cones in our study areas (Figures 10–13). This is not surprising given that increased rates of colluvial sediment transport will cause cone slope angles to lower more rapidly. Also, the spacing of first-order valleys in steady state landscapes [e.g., *Perron et al.*, 2008] and the spacing of channels in nonsteady state landscapes [e.g., *Simpson and Schlunegger*, 2003] have both been shown to increase as the magnitude of colluvial sediment transport processes increases relative to that of slope-wash/fluvial processes. Colluvial (diffusive) sediment transport mechanisms tend to smooth channel-like features that develop as a result of fluvial erosion. Decreases in K/D on south-facing hillslopes, all other factors remaining equal, can be expected to lead to an increase in the spacing between channels on those hillslopes relative to north-facing hillslopes (Figures 5f, 11, and 13). Numerical model results,

however, also show that the same asymmetries may occur as a result of multiple processes operating simultaneously. Higher values of K on north-facing hillslopes, in addition to higher values of D on south-facing hillslopes, further promote increases in drainage density on north-facing hillslopes relative to south-facing hillslopes. Variations in K may contribute to both hillslope asymmetry and differences in drainage density on opposing hillslopes (Figures 12 and 13b) but are not necessary to generate those landscape characteristics on cinder cones (Figures 10 and 11a).

The observation that asymmetries in hillslope angle and drainage density are strongly associated with a spatial variation in D does not address the underlying processes responsible for driving variations in D. The consistent relationship observed between NDVI and northness within all four volcanic fields demonstrates that the microclimatic effects associated with slope aspect are significant enough to influence vegetation growth in our study areas (Figures 5 and 6). In interpreting hillslope asymmetry within our study areas, we assume that floral bioturbation (e.g., tree-throw and root growth/decay) accounts for the majority of colluvial sediment transport and that rates of colluvial sediment transport increase with increasing vegetation cover/NDVI. These assumptions are consistent with studies that associate higher values of D with forested ecosystems [*Roering et al.*, 2002, 2004; *Hughes et al.*, 2009] and argue that disturbance-driven processes, such as tree-throw and root growth/decay, may dominate soil transport over geomorphic timescales [*Roering et al.*, 2002; *Hughes et al.*, 2009]. In particular, *Hughes et al.* [2009] argued that a change from grass/shrub-dominated vegetation during the late Pleistocene to forest colonization during the Holocene led to a near doubling of colluvial sediment fluxes at their study site near the Charwell River, South Island, New Zealand.

The notion that rates of colluvial sediment transport increase with increasing vegetation cover stands in contrast to the oft-cited idea that increases in vegetation cover serve to stabilize soil and suppress erosion. However, it is important to clearly distinguish between erosion by colluvial processes and erosion by slope-wash/fluvial processes in the context of this debate. Rates of slope-wash/fluvial erosion certainly increase with reductions in vegetation cover, all else being equal. However, cone hillslopes are likely to be dominated by colluvial transport processes due to the coarse (i.e., gravel dominated) and highly porous nature of their soils, at least initially. More generally, *Perron et al.* [2008, 2009] have shown that valley heads represent a transition from predominantly colluvial transport processes (on hillslopes) to slope-wash/fluvial transport processes (within and downstream from valley heads). As such, we can infer that slope-wash/fluvial processes are of lesser importance than colluvial transport processes on cones with little drainage development. Vegetation cover may also influence the angle of stability, S_c, in the nonlinear transport relationship that quantifies colluvial transport. A higher value of S_c can be expected to result in lower rates of colluvial sediment transport. If the primary effect of vegetation cover is to increase S_c by vegetative anchoring of soils, we would expect north-facing hillslopes to have lower topographic gradients (i.e., the opposite of what we observe) in the SFVF and SVF relative to south-facing hillslopes because north-facing hillslopes experienced less vegetation cover over the cooler and wetter climatic conditions prevalent during most of the lifetimes of the cones we studied in those fields (Figure 6). In addition, we would expect to see more pronounced topographic asymmetry on younger cones (in all four study areas), where the ratio of the average hillslope gradient to S_c is high in comparison to that found on older cinder cones. For these reasons, we associate our inferred increase in colluvial transport rates on south-facing hillslopes with a higher value of the colluvial transport coefficient, D, relative to north-facing hillslopes over the lifetime of the studied cinder cones.

In the SFVF and SVF, we hypothesize that this increase in D is the result of south-facing hillslopes having supported more vegetation cover than north-facing hillslopes during the majority of the Quaternary (Figure 6) and that this greater time-averaged vegetation cover led to an increased rate of floral bioturbation. Although not necessary to reproduce the hillslope/drainage density asymmetries observed in our study areas, less vegetation on north-facing hillslopes, throughout the lifetime of the cinder cones, may have also lead to spatial variations in K. Higher rates of slope-wash/fluvial erosion are often associated with environments having less vegetation [e.g., *Prosser and Dietrich*, 1995; *Prosser and Soufi*, 1998]. Model-predicted cinder cones produced with a higher K value on north-facing hillslopes and a higher D value on south-facing hillslopes had landscape characteristics consistent with the cinder cones in our study areas. That said, more research is needed to quantify how vegetation cover drives rates of colluvial and slope-wash/fluvial transport in different climatic regimes and among different vegetation types. Our interpretations are partially based on the assumption that rates of floral bioturbation increase with mean biomass. However, rates of

root growth/decay and vegetation turnover, which can be directly related to rates of floral bioturbation [*Gabet et al.*, 2003], may not necessarily increase with mean biomass. Therefore, it is difficult to rule out the alternative conceptual model that a greater colluvial transport coefficient on south-facing hillslopes is the result of higher rates of vegetation turnover on those hillslopes relative to north-facing hillslopes. Variations in the rate of vegetation turnover could have occurred regardless of whether mean biomass has been higher or lower on south-facing hillslopes relative to north-facing hillslopes.

There is also a growing body of evidence to suggest that variations in the frequency of freeze-thaw cycles with slope aspect is the primary cause of hillslope asymmetry in some environments [*Anderson et al.*, 2013; *West et al.*, 2014]. In a recent study of three watersheds in central Pennsylvania, *West et al.* [2014] concluded that gentler south-facing hillslopes at their study sites resulted from a higher frequency of freeze-thaw cycles on those hillslopes relative to north-facing hillslopes. The apparent increase in D on south-facing hillslopes in our study areas could also be explained by a higher frequency of freeze-thaw cycles on those hillslopes throughout the Quaternary relative to north-facing hillslopes. Such an effect could have occurred either from north-facing hillslopes remaining frozen for extended periods of time or from increased shielding of north-facing hillslopes due to more persistent snow cover. However, in the SFVF and SVF, we favor the hypothesis that the inferred increase in D on south-facing hillslopes is the result of increased floral bioturbation on those hillslopes because (1) bioturbation is likely the dominant form of colluvial sediment transport at these sites, particularly early in the life of these cones when the water-holding capacity of the soils (required for freeze-thaw-driven creep) is minimal, and (2) there is evidence to suggest that south-facing hillslopes supported more vegetation cover than north-facing hillslopes throughout the majority of the Quaternary within those volcanic fields (Figure 6).

Hillslope asymmetry on cinder cones in the NVF and MLVF also appears to be the result of slope-aspect-driven variations in the magnitude of colluvial sediment transport that persisted throughout the majority of the Pleistocene. Cinder cones in the NVF and MVLF, which are located at lower elevations and higher latitudes than the Arizona sites, may have undergone similar transitions from greater vegetation cover on south-facing hillslopes during LGM to greater vegetation cover on north-facing hillslopes in the present climate. It is likely that present-day patterns between northness and vegetation cover do not reflect the true relationship over the lifetime of the these cinder cones since large shifts in the upper tree line have occurred in the area near Grass Lake, located $\approx$ 50 km west of the MLVF at an elevation of 1500 m, within the last 40 kyr [*Hakala and Adam*, 2004]. Still, we currently lack the paleovegetation data required to test the hypothesis that greater vegetation cover on south-facing hillslopes throughout the majority of the Quaternary is responsible for the inferred increase in D on south-facing hillslopes in the NVF and MLVF. While this is one possible explanation, as is the idea that south-facing hillslopes experienced greater rates of vegetation turnover relative to north-facing hillslopes, freeze-thaw processes may also be the primary cause of the asymmetries. In high latitude areas such as the NVF and MLVF, freeze-thaw processes may be more important than floral bioturbation in setting rates of colluvial sediment transport. If this were the case, steeper north-facing hillslopes could be the result of a lower frequency of freeze-thaw cycles on those hillslopes relative to south-facing hillslopes over the lifetime of the cones.

Our results support those of other studies [e.g., *Poulos et al.*, 2012] that suggest both climate and elevation, which greatly influence the relative importance of different sediment transport mechanisms as well as the sensitivity of those mechanisms to climate, exert a strong control on the response of hillslope form to changes in microclimate. In water-limited areas, there may be a particular altitudinal range across which vegetation type/density changes rapidly and increases in moisture availability with increasing northness may lead to hillslope asymmetry within that range of elevations. In environments where colluvial sediment transport is dominated by freeze-thaw processes, hillslope asymmetry may develop at locations where slope aspect significantly influences the number of freeze-thaw cycles [e.g., *West et al.*, 2014]. At higher elevation or higher latitude, hillslope asymmetry may be the result of hillslope-aspect-driven variations in the dominance of glacial and nonglacial erosion mechanisms [*Naylor and Gabet*, 2007].

One of the major difficulties of using the presence of hillslope asymmetry to study interactions among climate and sediment transport processes is the inability to isolate the factors that affect asymmetry. Cinder cones represent an exceptionally well-constrained natural experiment for the study of hillslope asymmetry because they are relatively homogenous in terms of composition, can have known age constraints and initial conditions, and are present in large numbers within many different types of environments. Complex

interactions among slope aspect, soil development, grain size, and rates of colluvial sediment transport, which are beyond the scope of this study, may also influence rates of sediment transport and the magnitude (or presence) of topographic asymmetry on cinder cones. We focus on the role of vegetation and its connection with *D* since cinder cone degradation in our study areas is likely dominated by colluvial sediment transport processes and recent studies attest to the high relative importance of floral bioturbation in setting rates of colluvial sediment transport in forested ecosystems [*Roering et al.*, 2002; *Hughes et al.*, 2009].

7. Conclusions

Mean and maximum hillslope angles are similar on the north- and south-facing sides of young cinder cones within our study areas. However, north-facing hillslopes are steeper on older cinder cones within all four volcanic fields. Drainage density is higher on north-facing hillslopes relative to south-facing hillslopes. Results suggest that topographic asymmetry occurs within the studied cinder cone fields as a result of slope-aspect-driven differences in the magnitude of post-eruption sediment transport processes. Numerical model predictions suggest that observed asymmetries can be linked to an increase in the colluvial transport coefficient (i.e., the colluvial transport rate per unit hillslope gradient) on south-facing hillslopes relative to north-facing hillslopes. The age of the studied cinder cones suggests that present-day asymmetries may be better interpreted within the context of glacial climatic conditions. By analyzing present-day vegetation cover as a function of slope aspect and elevation, we argue that south-facing hillslopes maintained greater vegetation cover during the majority of the Quaternary in the SFVF and SVF. We attribute gentler south-facing hillslopes within the SFVF and SVF to greater rates of colluvial sediment transport caused by increased floral bioturbation on those hillslopes. We hypothesize that hillslope asymmetry on cinder cones in the NVF and MLVF also resulted from slope-aspect-driven variations in colluvial sediment flux that existed throughout the majority of the Quaternary.

Acknowledgments
We wish to thank Editor Alexander Densmore, Associate Editor Nicole Gasparini, and three anonymous reviewers for their detailed and constructive reviews.

References

Anderson, R. S. (1993), A 35,000 year vegetation and climate history from Potato Lake, Mongollon Rim, Arizona, *Quat. Res.*, *40*, 351–359.
Anderson, R. S., J. L. Betancourt, J. L. Mead, R. H. Hevly, and D. P. Adam (2000), Middle- and late-Wisconsin paleobotanic and paleoclimatic records from the southern Colorado Plateau, USA, *Palaeogeogr. Palaeoclimatol. Palaeoecol.*, *155*, 31–57.
Anderson, R. S., S. P. Anderson, and G. E. Tucker (2013), Rock damage and regolith transport by frost: An example of climate modulation of the geomorphology of the critical zone, *Earth Surf. Processes Landforms*, *38*, 299–316.
Bass, N. W. (1929), The geology of Cowley County, Kansas, *Kansas Geol. Surv. Bull.*, *12*, 9–23.
Betancourt, J. L. (1990), Late Quaternary biogeography of the Colorado Plateau, in *Packrat Middens—The last 40,000 Years of Biotic Change*, edited by J. L. Betancourt et al., pp. 259–293, Univ. of Ariz. Press, Tucson.
Branson, F. A., and L. M. Shown (1989), Contrasts of vegetation, soils microclimates, and geomorphic processes between north- and south-facing slopes on Green Mountain near Denver, Colorado, *U. S. Geol. Surv. Water-Resour. Invest. Rep., 89-4094*, pp. 1–18.
Burnett, B. N., G. A. Meyer, and L. D. McFadden (2008), Aspect-related microclimatic influences on slope forms and processes, northeastern Arizona, *J. Geophys. Res.*, *113*, F03002, doi:10.1029/2007JF000789.
Chitwood, L. A. (1994), Inflated basaltic lava—Examples of processes and landforms from central and southeast Oregon, *Oregon Geol.*, *56*(1), 11–21.
Churchill, R. R. (1981), Apsect-related differences in badlands slope morphology, *Ann. Assoc. Am. Geogr.*, *71*(3), 374–388.
Cole, K. L. (1990), Reconstruction of past desert vegetation along the Colorado River using packrat middens, *Paleogeog. Paleoclim. Paleoecol.*, *76*, 349–366, doi:10.1016/0031-0182(90)90120-V.
Colman, S. M., J. P. Bradbury, and J. G. Rosenbaum (2004), Paleolimnology and paleoclimate studies in Upper Klamath Lake, Oregon, *J. Paleolimnol.*, *31*, 129–138.
Condit, C. D., L. S. Crumpler, and J. C. Aubele (1989), Patterns of volcanism along the along the southern margin of the Colorado Plateau: the Springerville field, *J. Geophys. Res.*, *94*(B6), 7975–7986, doi:10.1029/JB094iB06p07975.
Conway, F. M., C. B. Connor, B. E. Hill, C. D. Condit, K. Mullaney, and C. M. Hall (1998), Recurrence rates of basaltic volcanism in SP cluster, San Francisco volcanic field, Arizona, *Geology*, *26*(7), 655–658.
Crumpler, L. S., J. S. Aubele, and C. D. Condit (1994), Volcanoes and neotectonic characteristics of the Springerville volcanic field, Arizona, in *New Mexico Geological Society Guidebook, 45th Field Conference, Mogollon Slope, West-Central New Mexico and East-Central Arizona*, edited by R. M. Chamberlin et al., pp. 147–164.
Cox, R. T. (1994), Analysis of drainage-basin symmetry as a rapid technique to identify areas of possible Quaternary tilt-block tectonics: An example from the Mississippi Embayment, *Geol. Soc. Am. Bull.*, *106*(5), 571–581.
Dohrenwend, J. C. (1978), Systematic valley asymmetry in the central California Coast Ranges, *Geol. Soc. Am. Bull.*, *89*, 891–900.
Dohrenwend, J. C., S. G. Wells, and B. D. Turrin (1986), Degradation of Quaternary cinder cones in the Cima Volcanic field, Mojave Desert, California, *Geol. Soc. Am. Bull.*, *97*, 421–427.
Donnelly-Nolan, J. M. (2006), Geologic map of medicine lake volcano, northern California, *U. S. Geol. Surv. Sci. Invest. Map, 2927*, scale 1:50,000.
Donnelly-Nolan, J. M., and M. A. Lanphere (2005), Argon dating at and near Medicine Lake volcano, California: Results and data, *U. S. Geol. Surv. Open-File Rep., 20051416*, pp. 1–37.
Emery, K. O. (1947), Asymmetrical valleys of San Diego county, California, *Bull. South. Calif. Acad. Sci.*, *46*(2), 61–71.
Fornaciai, A., M. Favalli, D. Karatson, S. Tarquini, and E. Boschi (2012), Morphometry of scoria cones, and their relation to geodynamic setting: A DEM-based analysis, *J. Volcanol. Geotherm. Res.*, *217-218*, 56–72.

Gabet, E. J., O. J. Reichman, and E. W. Seabloom (2003), The effects of bioturbation on soil processes and sediment transport, *Annu. Rev. Earth Planet. Sci.*, *31*(31), 249–273, doi:10.1146/annurev.earth.31.100901.141314.
Gesch, D. B. (2007), The National Elevation Dataset, in *Digital Elevation Model Technologies and Applications: The DEM Users Manual*, 2nd ed, edited by D. Maune, pp. 99–118, American Society for Photogrammetry and Remote Sensing, Bethesda, Maryland.
Gesch, D., M. Oimoen, S. Greenlee, C. Nelson, M. Steuck, and D. Tyler (2002), The national elevation dataset, *Photogramm. Eng. Remote Sens.*, *68*(1), 5–11.
Guittiérrez-Jurado, H. A., and E. R. Vivoni (2013), Ecogeomorphic expressions of an aspect-controlled semiarid basin: II. Topographic and vegetation controls on solar irradiance, *Ecohydrology*, *6*, 24–37, doi:10.1002/eco.1263.
Hack, J. T., and J. C. Goodlett (1960), Geomorphology and forest ecology of a mountain region in the Central Appalachian, *U. S. Geol. Surv. Prof. Pap., 347*, pp. 1–77.
Hakala, K. J., and D. P. Adam (2004), Late Pleistocene vegetation and climate in the southern Cascade Range and the Modoc Plateau region, *J. Paleolimnol.*, *31*, 189–215.
Hanks, T. C. (2000), The age of scarplike landforms from diffusion equation analysis, in *Quaternary Geochronology: Methods and Applications*, vol. 4, edited by J. S. Noller, J. M. Sowers, and W. R. Lettis, pp. 313–338, *Ref. Shelf*, AGU, Washington, D. C.
Hasenaka, T., and I. S. E. Carmichael (1985), The cinder cones of Michoacan-Guanajuato central Mexico: Their age, volume and distribution, and magma discharge rate, *J. Volcanol. Geotherm. Res.*, *25*, 105–124.
Heimsath, A. M., W. E. Dietrich, K. Nishiizumi, and R. C. Finkel (1997), The soil production function and landscape equilibrium, *Nature*, *388*, 358–361, doi:10.1038/41056.
Heimsath, A. M., W. E. Dietrich, K. Nishiizumi, and R. C. Finkel (1999), Cosmogenic nuclides, topography, and the spatial variation of soil depth, *Geomorphology*, *27*, 151–172, doi:10.1016/S0169-555X(98)00095-6.
Heimsath, A. M., W. E. Dietrich, K. Nishiizumi, and R. C. Finkel (2001), Stochastic processes of soil production and transport: Erosion rates, topo- graphic variation and cosmogenic nuclides in the Oregon Coast Range, *Earth Surf. Processes Landforms*, *26*, 531–552, doi:10.1002/esp.209.
Hildreth, W. (2007), Quaternary magmatism in the Cascades: Geologic perspectives, *U. S. Geol. Surv. Prof. Pap. 1744*, pp. 1–136.
Hooper, D. M. (1994), Geomorphologic modeling of the degradation evolution of scoria cones, PhD dissertation, Dep. of Geol., State Univ. of New York at Buffalo, Buffalo.
Hooper, D. M., and M. F. Sheridan (1998), Computer-simulation models of scoria cone degradation, *J. Volcanol. Geotherm. Res.*, *83*, 241–267.
Howard, A. D. (1994), A detachment-limited model of drainage basin evolution, *Water Resour. Res.*, *30*(7), 2261–2285, doi:10.1029/94WR00757.
Howard, A. D. (1997), Badland morphology and evolution: Interpretation using a simulation model, *Earth Surf. Processes Landforms*, *22*, 211–227.
Hughes, M., P. Almond, and J. J. Roering (2009), Increased sediment transport via bioturbation at the last glacial-interglacial transition, *Geology*, *37*, 919–922, doi:10.1130/G30159A.1.
Istanbulluoglu, E., O. Yetemen, E. R. Vivoni, H. A. Gutiérrez-Jurado, and R. L. Bras (2008), Eco-geomorphic implications of hillslope aspect: Inferences from the analysis of landscape morphology in central New Mexico, *Geophys. Res. Lett.*, *35*, L14403, doi:10.1029/2008GL034477.
Jefferson, A., G. E. Grant, S. L. Lewis, and S. T. Lancaster (2010), Coevolution of hydrology and topography on a basalt landscape in the Oregon Cascade Range, USA, *Earth Surf. Processes Landforms*, *35*, 803–816.
Jensen, R. A. (1988), *Roadside Guide to the Geology of Newberry Volcano*, CenOreGeoPub, Bend, Oregon.
Keith, W. J., H. D. King, M. E. Gettings, and F. L. Johnson (1988), Mineral resources of the devil's garden lava bed and four craters lava bed wilderness areas, Lake County, Oregon, *U. S. Geol. Surv. Bull., 1738-A*, pp. 1–24.
Lamb, M. P., M. Levina, R. A. DiBiase, and B. M. Fuller (2013), Sediment storage by vegetation in steep bedrock landscapes: Theory, experiments, and implications for postfire sediment yield, *J. Geophys. Res. Earth Surf.*, *118*, 1147–1160, doi:10.1002/jgrf.20058.
Leeder, M. R., and J. Alexander (1987), The origin and tectonic significance of asymmetrical meander-belts, *Sedimentology*, *34*, 217–226.
MacLeod, N. S., D. R. Sherrod, L. A. Chitwood, and R. A. Jensen (1995), Geologic map of Newberry Volcano, Deschutes, Klamath, and Lake Counties, Oregon, *U. S. Geol. Surv. Misc. Invest. Map, I-2455*, scales 1:62,500 and 1:24,000.
Melton, M. A. (1957), An analysis of the relations among elements of climate, surface properties, and geomorphology, *Dept. Geol. Columbia Univ. Tech. Rep.11, Proj. NR 389-042*, Off. of Nav. Res., New York.
Melton, M. A. (1960), Intravalley variation in slope angles related to microclimate and erosional environment, *Bull. Geol. Soc. Am.*, *71*(2), 133–144, doi:10.1130/0016-7606(1960)71[133:IVISAR]2.0.CO;2.
Molotch, N. P., M. T. Colee, R. C. Bales, and J. Dozier (2005), Estimating the spatial distribution of snow water equivalent in an alpine basin using binary regression tree models: The impact of digital elevation data and independent variable selection, *Hydrol. Processes*, *19*(7), 1459–1479, doi:10.1002/hyp.5586..
Moore, R. B., and E. W. Wolfe (1987), Geologic map of the east part of the San Francisco Volcanic Field, north-central Arizona, *U. S. Geol. Surv. Misc. Field Stud. Map, MF-1960, scale 1:50, 000*.
Naylor, S., and E. J. Gabet (2007), Valley asymmetry and glacial versus nonglacial erosion in the Bitterroot Range, Montana, USA, *Geology*, *35*(4), 375–378, doi:10.1130/G23283A.1.
Pelletier, J. D. (2008), *Quantitative Modeling of Earth Surface Processes*, Cambridge Univ. Press, New York.
Pelletier, J. D. (2013), A robust two-parameter method for drainage network extraction from high-resolution DEMs: Evaluation using synthetic and real-world DEMs, *Water Resour. Res.*, *49*, 75–89, doi:10.1029/2012WR012452.
Pelletier, J. D., and M. L. Cline (2007), Nonlinear slope dependent sediment transport in cinder cone evolution, *Geology*, *35*, 1067–1070.
Perron, J. T. (2011), Numerical methods for nonlinear hillslope transport laws, *J. Geophys. Res.*, *116*, F02021, doi:10.1029/2010JF001801.
Perron, J. T., W. E. Dietrich, and J. W. Kirchner (2008), Controls on the spacing of first-order valleys, *J. Geophys. Res.*, *113*, F04016, doi:10.1029/2007JF000977.
Perron, J. T., J. W. Kirchner, and W. E. Dietrich (2009), Formation of evenly spaced ridges and valleys, *Nature*, *460*, 502–505, doi:10.1038/nature08174.
Petit, J. R., et al. (1999), Climate and atmospheric history of the past 420,000 years from the Vostok Ice Core, Antarctica, *Nature*, *399*, 429–436.
Phillips, F. M., L. A. Peeters, M. K. Tansey, and S. N. Davis (1986), Paleoclimatic inferences from an isotopic investigation of groundwater in the central San Juan basin, New Mexico, *Quat. Res.*, *26*(2), 179–193, doi:10.1016/0033-5894(86)90103-1.
Pierce, K. L., and S. M. Colman (1986), Effect of height and orientation (microclimate) on geomorphic degradation rates and processes, late-glacial terrace scarps in central Idaho, *Geol. Soc. Am. Bull.*, *97*, 869–885.

Pouliquen, O. (1999), Scaling laws in granular flows down rough inclined planes, *Phys. Fluids*, *11*, 542–548, doi:10.1063/1.869928.
Poulos, M. J., J. L. Pierce, A. N. Flores, and S. G. Benner (2012), Hillslope asymmetry maps reveal widespread, multi-scale organization, *Geophys. Res. Lett.*, *39*, L06406, doi:10.1029/2012GL051283.
PRISM Climate Group (2004), Oregon State University. [Available at: http://prism.oregonstate.edu, created 4 Feb 2004.]
Prosser, I. P., and W. E. Dietrich (1995), Field experiments on erosion by overland flow and their implication for a digital terrain model of channel initiation, *Water Resour. Res.*, *31*, 2867–2876, doi:10.1029/95WR02218.
Prosser, I. P., and M. Soufi (1998), Controls on gully formation following forest clearing in a humid temperature environment, *Water Resour. Res.*, *34*, 3661–3671, doi:10.1029/98WR02513.
Rech, J. A., R. W. Reeves, and D. M. Hendricks (2001), The influence of slope aspect on soil weathering processes in the Springerville volcanic field, Arizona, *Catena*, *43*, 49–62.
Reeves, R. (1996), Cinder cones and the valley asymmetry problem, Association of American Geographers Annual Meeting, Abstract Volume.
Roering, J. J., J. W. Kirchner, and W. E. Dietrich (1999), Evidence for nonlinear, diffusive sediment transport on hillslopes and implications for landscape morphology, *Water Resour. Res.*, *35*(3), 853–870, doi:10.1029/1998WR900090.
Roering, J. J., P. Almond, P. Tonkin, and J. McKean (2002), Soil transport driven by biological processes over millennial time scales, *Geology*, *30*(12), 1115–1118, doi:10.1130/0091-7613(2002)030<1115:STDBBP>2.0.CO;2.
Roering, J. J., P. Almond, P. Tonkin, and J. McKean (2004), Constraining climatic controls on hillslope dynamics using a coupled model for the transport of soil and tracers: Application to loess-mantled hillslopes, Charwell River, South Island, New Zealand, *J. Geophys. Res.*, *109*, F01010, doi:10.1029/2003JF000034.
Russell, R. J. (1931), Geomorphological evidence of a climatic boundary, *Science*, *74*, 484–485.
Segerstrom, K. (1960), Erosion and related phenomena at Paricutin in 1957, *U.S. Geol. Surv. Bull. 1104-A*, U. S. Geol. Surv., Washington, D. C.
Settle, M. (1979), The structure and emplacement of cinder cone fields, *Am. J. Sci.*, *279*, 1089–1107.
Sexstone, G. A., and S. R. Fassnacht (2014), What drives basin scale spatial variability of snowpack properties in northern Colorado?, *Cryosphere*, *8*, 329–344.
Simpson, G., and F. Schlunegger (2003), Topographic evolution and morphology of surfaces evolving in response to coupled fluvial and hillslope sediment transport, *J. Geophys. Res.*, *108*(B6), 2300, doi:10.1029/2002JB002162.
Starratt, S. W., J. A. Barron, T. Kneeshaw, R. L. Phillips, J. L. Bischoff, J. B. Lowenstern, and J. A. Wanket (2003), A Holocene record from Medicine Lake, Siskiyou County, California: Preliminary diatom, pollen, geochemical, and sedimentological data, in *Proceedings of the Nineteenth Annual Pacific Climate Workshop*, edited by G. J. West, and N. L. Blomquist, pp. 131–147, Pacific Grove, Calif.
Stensrud, D. J. (2007), *Parameterization Schemes: Keys to Understanding Numerical Weather Prediction Models*, Cambridge Univ. Press, New York.
Stute, M., J. F. Clark, P. Schlosser, and W. S. Broecker (1995), A 30,000 yr continental paleotemperature record derived from noble gasses dissolved in groundwater from the San Juan basin, New Mexico, *Quat. Res.*, *43*, 209–220, doi:10.1006/qres.1995.1021.
Tarboton, D. G. (1997), A new method for the determination of flow directions and upslope areas in grid digital elevation models, *Water Resour. Res.*, *33*(2), 309–319, doi:10.1029/96WR03137.
Taylor, S. B., J. H. Templeton, and D. E. L. Giles (2003), Cinder cone morphometry and volume distribution at Newberry Volcano, Oregon: Implications for age relations and structural control on eruptive process [Abstracts with Programs], *Geol. Soc. Am.*, *35*(6), 421.
Thornthwaite, C. W. (1931), The climates of North America according to a new classification, *Geog. Rev.*, *21*, 633–655.
Thorson, T. D., S. A. Bryce, D. A. Lammers, A. J. Woods, J. M. Omernik, J. Kagan, D. E. Pater, and J. A. Comstock (2003), *Ecoregions of Oregon (Color Poster with Map, Descriptive Text, Summary Tables, and Photographs)*, U. S. Geol. Surv., Reston, Virginia.
Tucker, G. E., and K. X. Whipple (2002), Topographic outcomes predicted by stream erosion models: Sensitivity analysis and intermodel comparison, *J. Geophys. Res.*, *107*(B9), 2179, doi:10.1029/2001JB000162.
Ulrich, G. E., and N. G. Bailey (1987), Geologic map of the SP Mountain part of the San Francisco volcanic field, north-central Arizona, *U. S. Geol. Surv. Misc. Field Stud. Map, MF-1956*, scale 1:50,000.
Wagner, J. D. M., J. E. Cole, J. W. Beck, P. J. Patchett, G. M. Henderson, and H. R. Barnett (2010), Moisture variability in the southwestern United States linked to abrupt glacial climate change, *Nat. Geosci.*, *3*, 110–113, doi:10.1038/NGEO707.
Walker, G. W., N. V. Peterson, and R. C. Greene (1967), Reconnaissance geologic map of the east half of the Crescent quadrangle, Lake, Deschutes, and Crook Counties, Oregon, *U. S. Geol. Surv. Misc. Geol. Invest. Map, I-493, scale 1:250,000*, scale 1:250,000.
West, N., E. Kirby, P. Bierman, and B. A. Clarke (2014), Aspect-dependent variations in regolith creep revealed by meteoric ^{10}Be, *Geology*, *42*, 507–510, doi:10.1130/G35357.1.
Wolfe, E. W., G. E. Ulrich, R. F. Holm, R. B. Moore, and C. G. Newhall, (1987), Geologic map of the central part of the San Francisco volcanic field, northcentral Arizona, *U. S. Geol. Surv. Misc. Field Stud. Map, MF-1959*, scale 1:50,000.
Wood, C. A. (1980a), Morphometric analysis of cinder cone degradation, *J. Volcanol. Geotherm. Res.*, *7*, 387–413.
Wood, C. A. (1980b), Morphometric analysis of cinder cone degradation, *J. Volcanol. Geotherm. Res.*, *8*, 137–160.
Zhu, C., and R. Kipfer (2010), Noble gas signatures of high recharge pulses and migrating jet stream in the late Pleistocene over Black Mesa, Arizona, United States, *Geology*, *38*(1), 83–86.